DOE/ET/51010--8

WFPS:TME-79-033
DECEMBER 31, 1979

MASTER

AN EXPERIMENTAL STUDY OF UNIPOLAR ARCS IN A LOW PRESSURE MERCURY DISCHARGE

CAROL T. JOHNSON

UNIVERSITY OF PITTSBURGH
DEPARTMENT OF ELECTRICAL ENGINEERING

COOPERATIVE GRADUATE EDUCATION PROGRAM IN FUSION TECHNOLOGY
ADMINISTERED FOR THE U.S. DEPARTMENT OF ENERGY
BY THE WESTINGHOUSE ELECTRIC CORPORATION
CONTRACT EG-77-C-02-4231-A000

DISCLAIMER

ACKNOWLEDGEMENT

This work was performed for the U.S. Department of Energy, under Contract EG-77-C-02-4231-A000, Cooperative Graduate Education Program in Fusion Technology. Reproduction, translation, publication, use and disposal, in whole or in part, by or for the United States Government is permitted.

The author would like to express her sincere appreciation to Mr. G. S. Smeltzer of the Westinghouse Fusion Power Systems Department and Dr. J. Falk of the University of Pittsburgh's Electrical Engineering Department for acting as her advisors on this project. Thanks also goes to Dr. A. E. Robson of the Naval Research Laboratory, Dr. A. Lee, Dr. C. W. Kimblin, Dr. J.V.R. Heberlein, Dr. G. L. Rogoff, Dr. J. W. McNall, and Dr. P. G. Slade, all of the Westinghouse Research and Development Center, Dr. F. M. Heck and Dr. D. Klein, both of the Westinghouse Fusion Power Systems Department, and Dr. A. Bishop of the University of Pittsburgh's Chemical Engineering Department, for their interest, scientific insight, and support. I would finally like to thank the Westinghouse Fusion Power Systems Department, the Westinghouse Research and Development Center, and the Department of Energy for their financial support of this project.

Printed in the United States of America
Available from

National Technical Information Service
U.S. Department of Commerce
5285 Port Royal Road
Springfield VA 22161

NTIS Price Codes
Printed Copy: A04
Microfiche Copy: A01

WFPS:TME-79-033
DECEMBER 31, 1979

AN EXPERIMENTAL STUDY OF UNIPOLAR ARCS IN A LOW PRESSURE MERCURY DISCHARGE

PREPARED BY: Carol T. Johnson
Carol T. Johnson
Graduate Student Program Participant
University of Pittsburgh

REVIEWED BY: F. M. Heck
F. M. Heck, Manager
Systems Engineering

APPROVED BY: T. C. Varljen
T. C. Varljen, Manager
Engineering

fusion power
systems department

Westinghouse Electric Corporation
P.O. Box 10864, Pgh. Pa. 15236

TABLE OF CONTENTS

		PAGE
	Abstract	1
I)	Introduction	2-3
II)	Theory	4-18
	A. Unipolar Arcs	4-11
	B. Double Langmuir Probes	11-18
	i) Floating Double-Probes	11-15
	ii) Saturation Ion Currents	15-16
	iii) Determination of T_e and n_e	16-18
III)	Experiment	19-29
	A. Discharge Tube	19
	B. RF Coupling and Plasma Initiation	19-24
	C. Switching Circuit and DC Arc Initiation	24-26
	D. Unipolar Arc Mode	26
	E. Probe Characteristics	26-29
	F. Data Collection	29
IV)	Results	30-34
	A. General Observations	30-31
	B. Unipolar Arc Data	31-34
	i) Unipolar Arc Current Waveforms	31-33
	ii) Variation of the Unipolar Arc Current with RF Power	33
	iii) Variation of the Unipolar Arc Current with Metal Plate Surface Area	33-34

TABLE OF CONTENTS (cont.)

		PAGE
V)	Discussion	35-43
	A. Unipolar Arcs	35-42
	i) The Sheath Voltage V_s	35-36
	ii) Negative Arc Voltages	36-38
	iii) Saturation Ion Currents	38-39
	iv) Unipolar Arc Current	39-41
	v) Surface Area Effects	41-42
	B. Alternative Arc Driving Mechanisms	43-44
	i) Full-Wave Rectification	43
	ii) Half-Wave Rectification	43
VI)	Conclusions and Recommendations	45-46

ABSTRACT

An experimental study of unipolar arcs was conducted in a low pressure mercury discharge inductively heated with RF. The results were found to be consistent with the concept of a sheath mechanism for driving the unipolar arcs. Floating double-probe measurements of the unipolar arc plasma parameters yielded electron temperatures of $\sim$2 eV and electron number densities of $\sim 1 \times 10^{11} cm^{-3}$ assuming quasi-neutral plasma conditions. The variation of the unipolar arc current with 1) the RF power input and 2) the metal surface area exposed to the plasma verified the predicted dependence of the arc current on the plasma parameters and the metal surface area. Finally, alternative mechanisms for sustaining the observed arcs by high frequency rectification were ruled out on the basis of the recorded current waveforms of the unipolar arcs.

I) INTRODUCTION

Plasma-wall interactions in fusion reactors produce high-Z impurities as a result of erosion of the first wall. The concentrations of these impurities may be sufficient[1] to effectively cool the plasma through radiation and thus quench the fusion reaction. Arc trails of both linear and fern-like configurations (Figure 1) found in DITE,[2-6] PLT,[7] Macrotor,[8] TFR,[9] and ZETA[10] indicate that some form of arcing is occurring along with blistering and sputtering. Unipolar arcs have been suggested as one of the possible arcing mechanisms contributing to this erosion process.

Unipolar arcs were first described by Robson and Thonemann[10] in 1959 for a low pressure mercury discharge in which an arc spot was supported on a metal surface next to a highly ionized plasma. This paper claimed that the arcs were driven by a sheath potential set up between an isolated metal wall and the plasma. Since that time many questions have been raised about the concept of unipolar arcs, their initiation mechanism, and the plasma conditions needed to support them. In this study, the initial experiment[10] of Robson and Thonemann was reproduced and extended to gather quantitative information on the nature of the plasma and the unipolar arc itself. The results were then compared with those predicted by the sheath theory.

In Section II, a brief description of the unipolar arc model[10] of Robson and Thonemann is presented, followed by a review of the floating double-probe theory. In Section III the present experiment is described in detail, and the results are presented in Section IV. Finally, a discussion of the results and the conclusions and recommendations are given in Sections V and VI respectively.

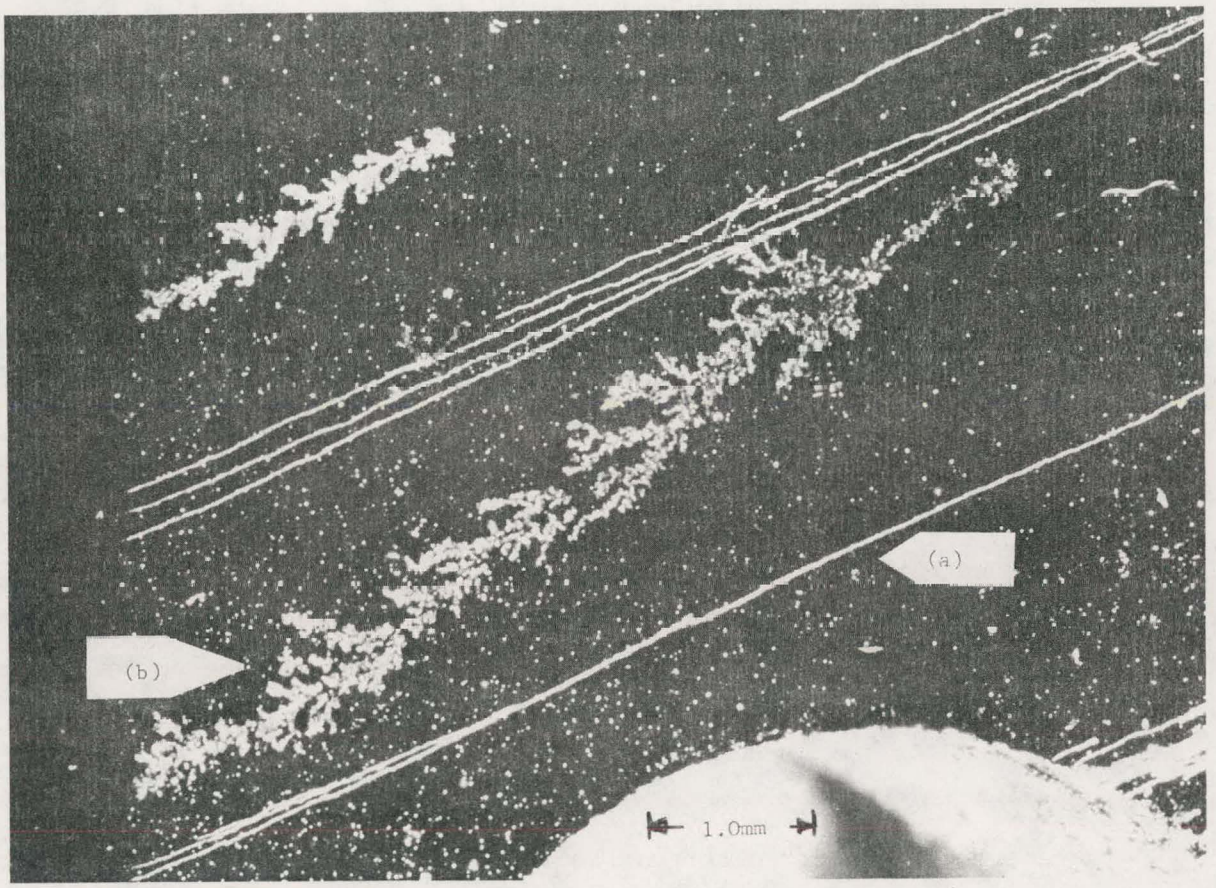

Figure 1. Linear (a) and Fern-Like (b) Arc Root Configurations Observed on the First Wall of the DITE Reactor (Ref. 2).

II) THEORY

A. Unipolar Arcs

Unipolar arcs are driven[10] by the potential drop in the sheath formed between a plasma and a floating metal wall. The arc current is made up of electrons that are emitted into the plasma from a localized cathode spot in the wall and returned to the wall by their random thermal motion (Figure 2). Since the wall thus acts to receive and emit electrons driven by this sheath potential the term unipolar arc was used for this phenomenon.

Given that a metal surface is exposed[10] to a plasma, electrons and ions will bombard that surface. Initially, if the plate is at the plasma potential, the electron current density j_e to the plate will be greater than the ion current density j_i due to the electron and ion random velocity differences. The surface will therefore become negatively charged with respect to the plasma until the potential difference between the plasma and the plate reaches the sheath potential V_s (Figure 2a). This potential acts to retard the electron flow to the surface so that

$$j_e + j_i = 0. \tag{1}$$

In general the electron current density j_e to a floating metal plate at potential V with respect to the plasma is

$$j_e = \frac{1}{4} n_e e \bar{v}_e e^{(-eV/kT_e)} \tag{2}$$

where

$$\bar{v}_e = (8kT_e/\pi m_e)^{1/2} . \tag{3}$$

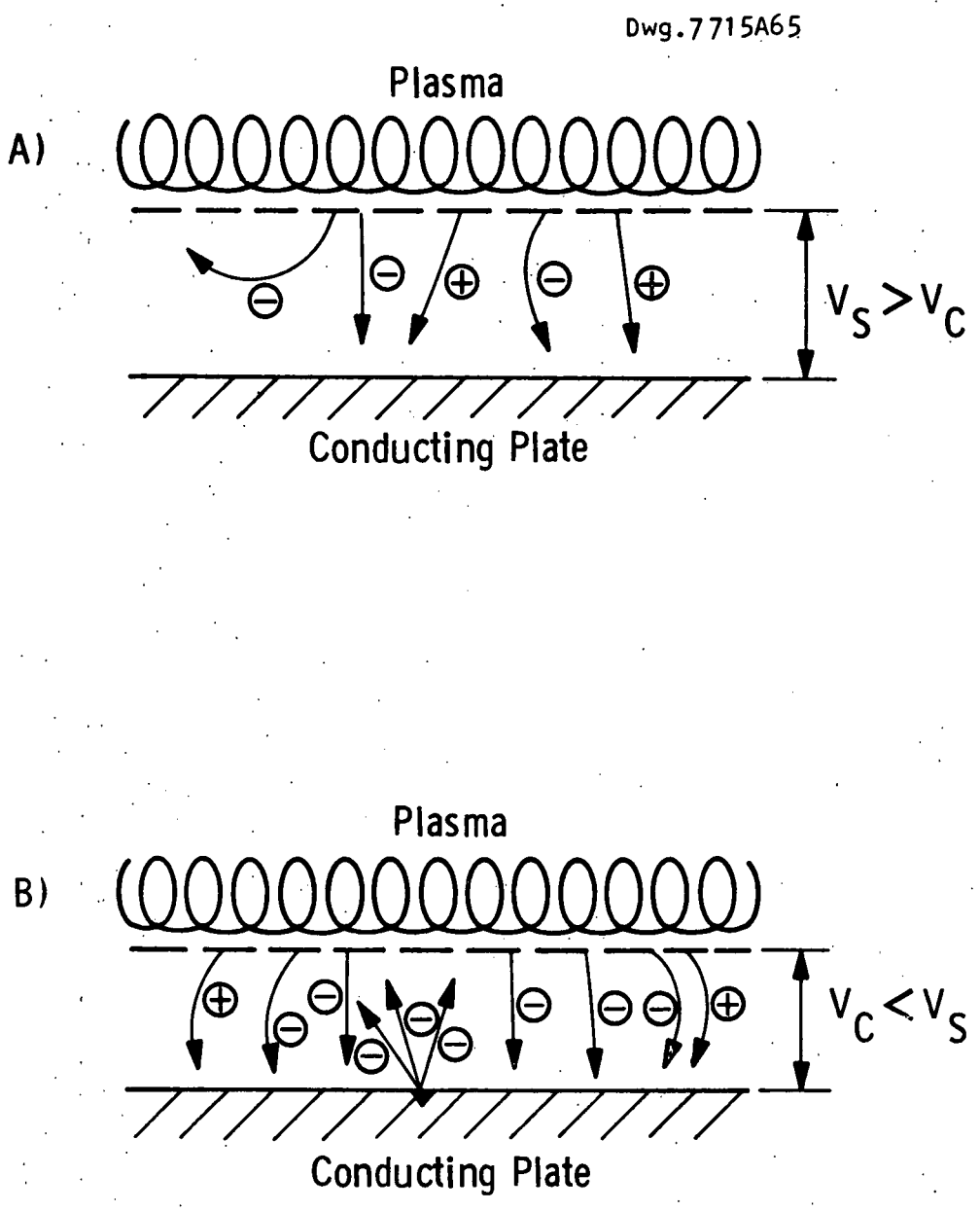

Figure 2. Unipolar Arc Sheath Mechanism (Ref.10).

The ion current density at the sheath boundary is given by

$$j_i = n_i e_i v_i \tag{4}$$

where

$$v_i = \gamma(kT_e/m_i)^{1/2} \tag{5}$$

$$\gamma \approx 1. \quad \text{(c.f. Ref. 11)} \tag{6}$$

The subscripts e and i refer to electron and ion, and

n_e, n_i = number densities

e, e_i = charges

$v_e . v_i$ = velocities

m_e, m_i = masses

T_e, T_i = temperatures

The velocity v_i is determined from the Bohm sheath criterion.[11] At the plane x = 0 (Figure 3) the ions enter the sheath region from the plasma with a drift velocity v_i. Assume $T_i = 0$ so that all ions have the velocity v_i at x = 0. (The unipolar arc plasma conditions are actually such that $T_i << T_e$ and not zero. The assumption that $T_i = 0$ simplifies the calculations. This restriction will be removed below. For low pressure discharges, the ions are essentially in thermal equilibrium with the neutrals which have a temperature slightly above room temperature. The particular low pressure discharge studied in this experiment was mercury). As in Figure 3 the potential V(x) in the planar sheath is assumed to decrease monotonically with x.

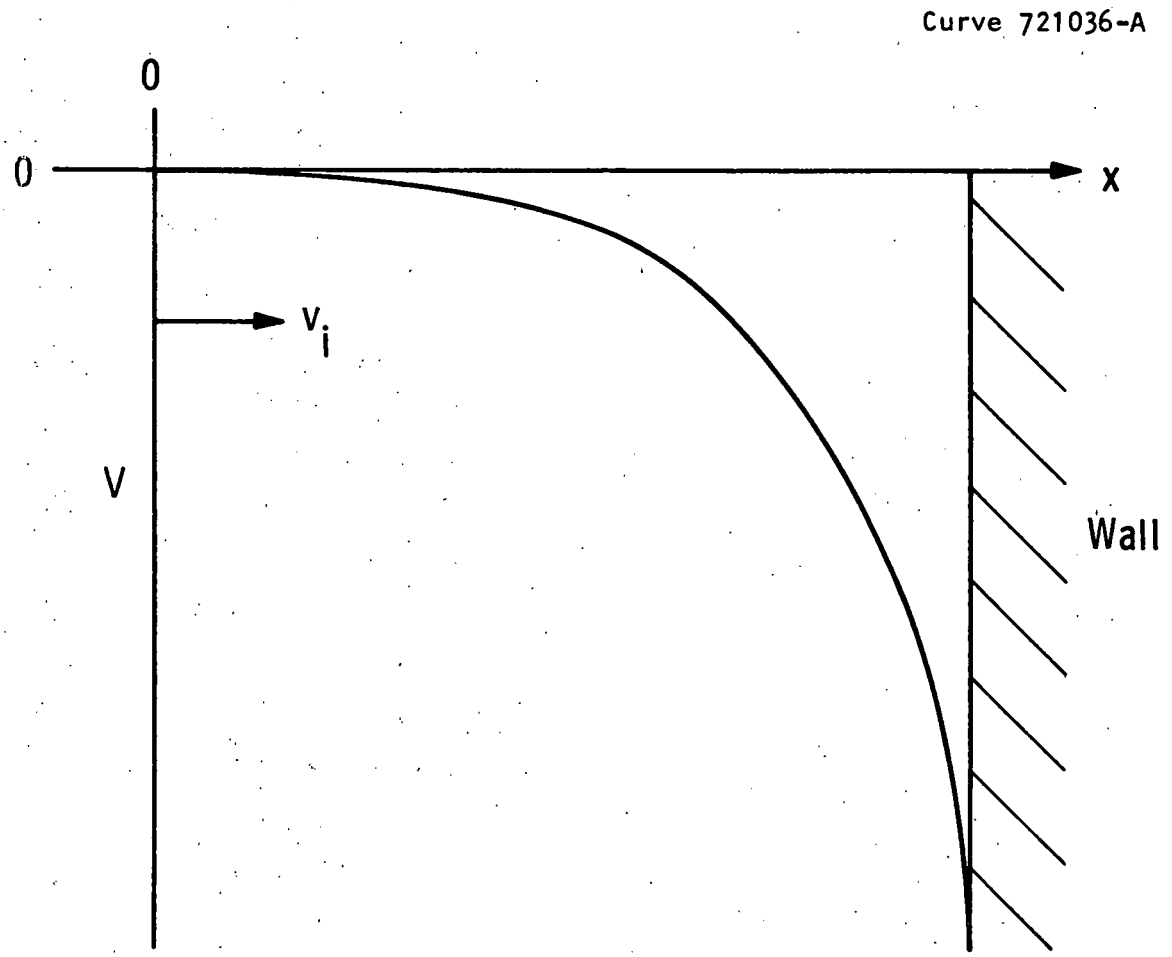

Figure 3. The potential V(x) in the planar sheath. The cold ions enter the sheath at the velocity v_i (Ref. 12).

The conservation of energy gives

$$\frac{1}{2} m_i v_i^2(x) = \frac{1}{2} m_i v_i^2 - e_i V(x) \tag{7}$$

$$v_i(x) = \left[v_i^2 - \frac{2e_i V(x)}{m_i} \right]^{1/2} \tag{8}$$

where $v_i(x)$ is the ion velocity at position x in the sheath. The $v_i = v_i(0)$. The ion continuity equation gives the ion density n_i in terms of the plasma density n_o. The plasma density is equal to the density of atoms that have been ionized. Therefore

$$n_o v_i = n_i(x) v_i(x) \tag{9}$$

and

$$n_i(x) = n_o \left[1 - \frac{2e_i V(x)}{m_i v_i^2} \right]^{-1/2} . \tag{10}$$

For a Maxwellian electron distribution with velocity components normal to the sheath, the electron density is

$$n_e = n_o \, e^{(-eV(x)/kT_e)} \tag{11}$$

Substitution of n_i and n_e into Poisson's equation results in

$$\frac{d^2V(x)}{dx^2} = 4\pi e_i (n_e - n_i) \tag{12}$$

$$= 4\pi e_i n_o \left[e^{e_i V(x)/kT_e} - \left[1 - \frac{2e_i V(x)}{m_i v_i^2} \right]^{-1/2} \right]. \tag{13}$$

Then simplifying Eq. 13 with the notation

$$\rho \equiv -e_i V(x)/kT_e \tag{14}$$

$$\beta = x\left[\frac{4\pi n_o e_i^2}{kT_e}\right]^{1/2} \tag{15}$$

$$\alpha = \frac{v_i}{(kT_e/m_i)^{1/2}} \tag{16}$$

gives

$$\rho'' = \left[1 - \frac{2\rho}{\alpha^2}\right]^{-1/2} - e^{-\rho} \tag{17}$$

where $\rho' = d\rho/d\beta$ and $\rho'' = d^2\rho/d^2\beta$.

Multiplying both sides by ρ' and integrating yields

$$\frac{1}{2}(\rho'^2 - \rho_o'^2) = \alpha^2\left[(1 + \frac{2\rho}{\alpha^2})^{1/2} - 1\right] + e^{-\rho} - 1 \tag{18}$$

since $\rho = 0$ at $\beta = 0$. If $\vec{E} = 0$ in the plasma so that $\rho_o' = 0$ at $\beta = 0$, the right-hand side of Eq. 18 then has to be positive for all of ρ. In particular, for $\rho << 1$ the Taylor series expansion of the right-hand side yields the result that

$$\frac{1}{2}\rho^2(-1/\alpha^2 + 1) > 0 \tag{19}$$

$$\alpha^2 > 1 \text{ or } v_i > \left[\frac{kT_e}{m_i}\right]^{1/2}. \tag{20}$$

This condition is known as the Bohm sheath criterion and says that the ions must enter the sheath region at a velocity greater than the ion acoustic velocity. If the ions have finite temperature, v_i will be somewhat lower. As a mean value the ion velocity becomes

$$v_i = \left[\frac{kT_e}{m_i}\right]^{1/2} \qquad (5)$$

Returning to the consideration of the sheath potential V_s, substituting Eqs. 2 and 4 into Eq. 1 gives

$$V_s = \frac{kT_e}{2e} \ln\left(\frac{m_i}{2\pi m_e}\right). \qquad (21)$$

If the electron temperature T_e is sufficiently high V_s will be greater than the minimum potential needed to sustain an arc. This potential is the cathode potential V_c. If a cathode spot is then somehow initiated on the metal surface the retarding potential will drop from V_s to V_c due to the strong local emission of electrons through the cathode spot (Figure 2b). The ion flux is assumed to be neglible. With the lowering of the retarding potential, more of the high energy electrons from the tail of the electron energy distribution will flow to the plate. In order to keep the total current to the plate zero (Eq. 1), the electrons hitting the plate in the vicinity of the cathode must equal those returning to the plasma through the cathode spot. The electrons make up the unipolar arc current I_c.

The arc current I_c can be calculated through the use of the above equations as follows. The arc current I_c is equal to

$$I_c = Aj_e + Aj_i \qquad (22)$$

$$= A\left[\frac{1}{4} n_e e \bar{v}_e \exp\left(\frac{-eV_c}{kT_e}\right) + n_i e_i v_i\right] \qquad (23)$$

where A is the surface area of the metal exposed to the plasma. The quasi-neutral plasma assumption is made and $n_o = n_i = n_e$. The definitions of j_e and j_i are taken from Eqs. 2 and 4 above. Using Eqs. 3 and 5 for the velocities yields

$$I_c = An_e e \left[-\left(\frac{kT_e}{m_i}\right)^{1/2} + \left(\frac{kT_e}{2\pi m_e}\right)^{1/2} \exp\left(\frac{-eV_c}{kT_e}\right)\right]. \tag{24}$$

Rearranging terms and using the sheath potential V_s gives

$$I_c = An_e e \left(\frac{kT_e}{2\pi m_e}\right)^{1/2} \left[\exp\left(\frac{-eV_c}{kT_e}\right) - \exp\left(\frac{-eV_s}{kT_e}\right)\right]. \tag{25}$$

Since for each type of cathode material there is a minimum arc current[9] needed to sustain the arc spot, a minimum plate area A exists to support that current for a given set of plasma conditions. In addition, the minimum electron temperature needed to fulfill the condition

$$V_s \geq V_c \tag{26}$$

for a given gas can be found using Eq. 21 if V_c is known. The cathode fall V_c of a mercury pool cathode is ~ 9 V[13] which gives a minimum electron temperature of 1.7 eV for a mercury plasma. For a hydrogen plasma the minimum T_e is 3.2 eV with a mercury pool cathode.

The mechanism whereby the cathode spot is initiated on a reactor's first wall is not understood. It has been suggested that imperfections[14-17] in the wall's surface give rise to high local fields at the metal surface that can cause breakdown. Ions accelerated by these fields bombard the wall to cause localized spots of high secondary electron emission that form cathode spots.

B. Double Langmuir Probes

i) Floating Double-Probes[18]

From Eq. 21 an important plasma parameter for the determination of the sheath potential V_s is T_e. With Langmuir double probes inserted

into the plasma, the electron temperature T_e along with the electron number density n_e can be measured if the plasma conditions are stable, the charged particles have approximately a Maxwellian distribution, and the mean free path is large compared to the probe or sheath dimensions. Knowledge of the electron number density n_e and the electron temperature T_e allows calculation of the sheath potential V_s (Eq. 21) and the arc current I_c (Eq. 25).

Electrostatic probes are small wires inserted into a plasma and electrically isolated from ground. Their dimensions are chosen so that their presence has a minimal effect on the plasma and thus the parameters they monitor. Cylindrical probe diameters are typically made comparable to the sheath thickness which may be several Debye lengths for the particular plasma conditions. Double probes are biased with respect to each other and insulated from ground (Figure 4b). When the differential probe voltage V is zero, the probes are at the floating potential V_f and no current flows between them. By applying a positive voltage V between probes 1 and 2

$$V = V_1 - V_2 > 0 \qquad (27)$$

a current I(V) flows between them. More electrons flow to 1 than 2 which results in a positive current from probe 2 to probe 1. The potential distribution shown in Figure 4a indicates, however, that both probes are always negative with respect to the plasma. The less negative probe draws a net electron current; the more negative probe draws a compensating net ion current which cannot exceed the ion saturation currents.

Consider the probe characteristic in Figure 5. In the case where V is positive, V_1 becomes less negative than the floating potential V_f so that it collects electrons. It does not reach the plasma potential V_P however. V_2, on the other hand, becomes more negative than the floating potential thus drawing ions. These currents are not independent of each other, but are coupled by Kirchhoff's law

Dwg.7715A62

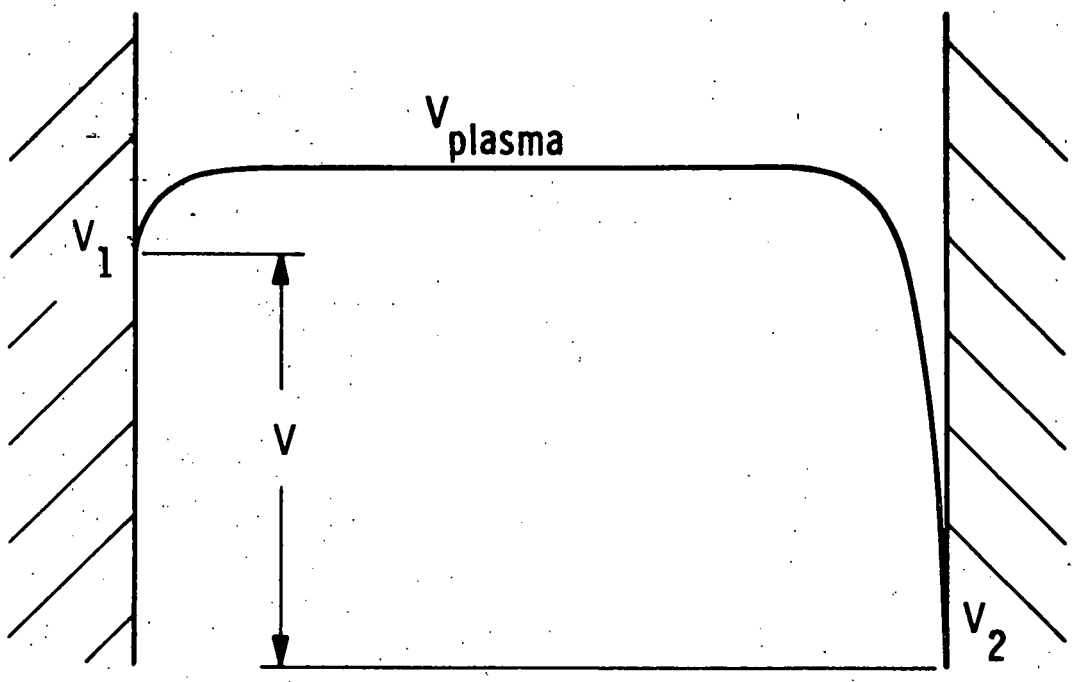

Figure 4a. Potential Distribution between the Probes of a Floating Double-Probe System (Ref. 18).

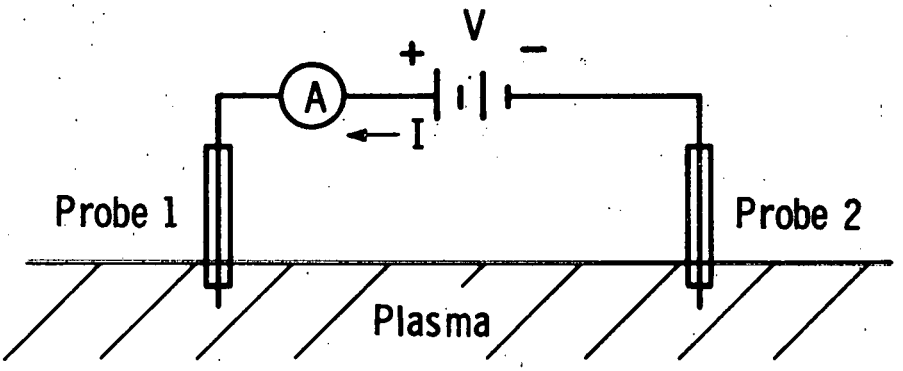

Figure 4b. Schematic of a Floating Double-Probe System Showing the Convention Used for the Sign of I (Ref. 18).

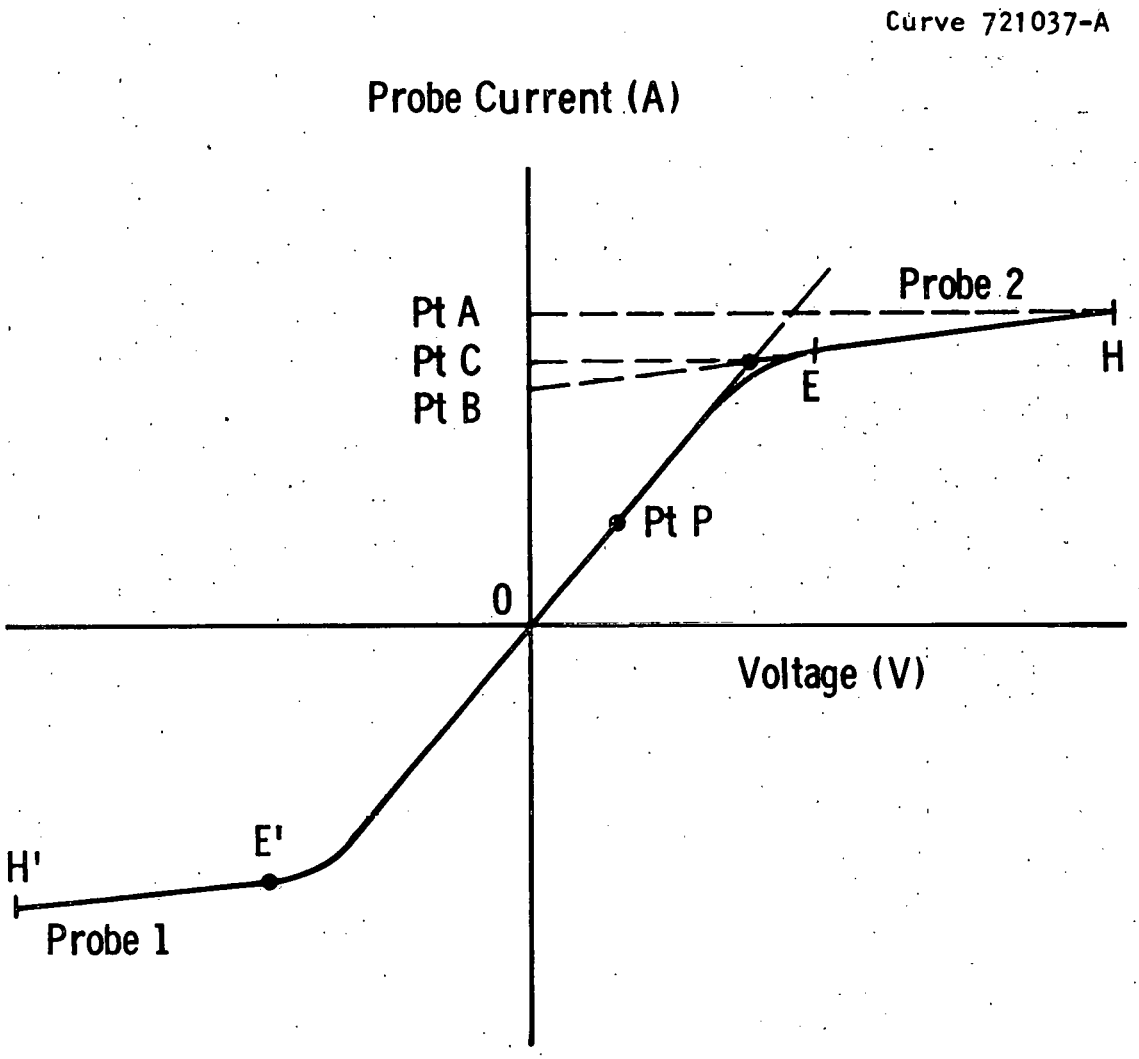

Figure 5. Probe Characteristic for Floating Double-Probe System. Probe surface areas are equal (Ref. 18).

$$I = i_{1-} - i_{1+} = i_{2+} - i_{2-} \tag{28}$$

where i_{1-}, i_{2-} are the respective electron currents and i_{1+}, i_{2+} are the respective ion currents to probes 1 and 2. The monitored current is shown as Pt. P in Figure 5. By then making V more positive, probe 2 becomes quite negative and collects the saturation ion current. Probe 1 being relatively close to the plasma potential collects enough electrons to cancel this ion current to probe 2. This is represented by the ion saturation regime EH of Figure 5. For V less than zero the roles of probes 1 and 2 are reversed as shown.

An advantage of the floating double-probe measurement is that the system never draws more than the saturation ion current. This minimizes the probes' effects on the system. Double probes also have a definite reference voltage. One disadvantage is that the electrons collected are from the high energy end of the energy distribution. They do not, therefore, necessarily reflect the behvaior of the bulk electrons accurately, unless the electrons are truly Maxwellian.

ii) Saturation Ion Currents

The basic assumption of this theory is that the probes are always negative enough to collect the ion saturation current. The ion saturation current I_{SAT} is given by

$$I_{SAT} = \frac{1}{2} A n_o e \left[\frac{kT_e}{m_i}\right] 1/2 \tag{29}$$

from the Bohm sheath theory.[12] For double probes of equal surface area the measured saturation ion currents of probe 1, i_{1+}, and probe 2, i_{2+}, are related to I_{SAT} by

$$I_{SAT} = i_{1+} = i_{2+} \tag{30}$$

if probes 1 and 2 have equal surface areas.

Several methods of interpreting the probe characteristics for i_{1+} and i_{2+} have been used.[18-20] One method[18] is to linearly extrapolate the line through EH (Figure 5) back to the y axis for i_{2+}. (See Pt. B) But this is felt[18] to give too low a value. The method used here is to take the ordinate of the asymptote intersection[20] of the probe transition and saturation regions. (Pt. C) Pt. A or the maximum current measured is also indicated as an evaluation point for comparison. The i_{1+} values are found in a similar manner.

The above discussion has applied to plasmas with a Maxwellian electron energy distribution. For plasmas with a non-Maxwellian distribution of several temperature components, the floating double-probe characteristic interpretation becomes more difficult. Such a temperature distribution could prevent the ion saturation region from assuming a fairly flat characteristic as shown in Figure 5 (Region EH) since I_{SAT} would not be a function of a single T_e (Eq. 29). The rate of rise of the current in this region could be significant with such plasma conditions. A steep slope causes the discrepancy between the current values at Pt. A, Pt. B and Pt. C to increase. For this reason single probe measurements would be an advantage since they register the various temperature components.[21] Such Langmuir probe studies in RF plasmas have been conducted.[21,22]

iii) Determination of T_e and n_e

From Kirchhoff's law

$$I = i_{1-} - i_{1+} = i_{2+} - i_{2-}. \qquad (28)$$

The electron current density in the transition region EE´ is given by

$$i_{1-} = A_1 j_r e^{(-eV_1/kT_e)} \qquad (31)$$

$$i_{2-} = A_2 j_r e^{(-eV_2/kT_e)} \qquad (32)$$

where V_1 and V_2 are negative, A_1 and A_2 are the respective probe areas and j_r is the random electron current density. From Eq. 28 and the assumption that the measured ion saturation current (i_{1+} or i_{2+}) is independent of V

$$\frac{dI}{dV} = \frac{di_{1-}}{dV} = -\frac{di_{2-}}{dV} . \tag{33}$$

Eq.'s 31, 32, and 33 give

$$A_1 j_r \left[e^{-eV_1/kT_e} \right] \frac{e}{kT_e} \frac{dV_1}{dV} + A_2 j_r \left[e^{-eV_2/kT_e} \right] \frac{e}{kT_e} \frac{dV_2}{dV} = 0. \tag{34}$$

By using Eq. 27

$$1 = \frac{dV_1}{dV} - \frac{dV_2}{dV} \tag{35}$$

Eq. 34 becomes

$$A_1 \left[e^{-eV_1/kT_e} \right] \frac{dV_1}{dV} + A_2 \left[e^{-eV_2/kT_e} \right] \left(\frac{dV_1}{dV} - 1 \right) = 0. \tag{36}$$

At V = 0, $V_1 = V_2$ and this gives

$$\left. \frac{dV_1}{dV} \right]_o = \frac{A_2}{A_1 + A_2} \tag{37}$$

from Eq. 36. Eq.'s 31, 33, and 37 give

$$\left. \frac{dI}{dV} \right]_o = -\frac{A_1 A_2}{A_1 + A_2} j_r \frac{e}{kT_e} e^{-eV_f/kT_e} \tag{38}$$

at V = 0. Since

$$j_+ = j_r e^{-eV_f/kT_e}, \tag{39}$$

where V_f is the floating potential of the probes, and $i_{1+} = A_1 j_+$ and $i_{2+} = A_2 j_+$

$$\left.\frac{dI}{dV}\right]_o = -\frac{e}{kT_e}\,\frac{i_{1+} \cdot i_{2+}}{i_{1+} + i_{2+}}\,. \tag{40}$$

The $\left.\frac{dI}{dV}\right]_o$ thus gives T_e by using the measured values of the ion saturation currents i_{1+} and i_{2+}. The electron number density can then be found from Eq. 29 for the ion saturation current

$$I_{SAT} = \frac{1}{2}\, An_o e\left[\frac{kT_e}{m_i}\right] 1/2 \tag{29}$$

since T_e is known through Eq. 40 and

$$I_{SAT} = i_{1+} = i_{2+} \tag{30}$$

The quasi-neutral plasma condition $n_0 = n_e = n_i$ is assumed.

III) EXPERIMENT

A. Discharge Tube

The mercury discharge tube (Figure 6) for the unipolar arc study was constructed of Pyrex with a diameter of 7 cm and a length of 22 cm. Three nickel plates (anodes) (6.0 cm x 4.7 cm x .08 cm) were positioned .75 cm from the inner wall of the tube as can be seen in Figure 7. The nickel surfaces were simply machine polished, cleaned with alcohol, and rounded at the corners. The mercury pool cathode with a nickel spot-anchor was located opposite the center plate with a mercury pool surface area of approximately 3 cm^3. The two Langmuir probes were 20 mil tungsten wire, inserted in the discharge tube, and separated by .5 cm. A length of .75 cm was exposed to the plasma.

In order to control the mercury vapor pressure a Plexiglas reservoir was constructed and glued around the outside of the cathode (Figure 6). Water was flushed through the cup to keep the cathode at a constant temperature which was monitored by a thermocouple. This procedure controlled the cold spot temperature of the discharge tube which in turn determined the mercury vapor pressure. Figure 8 gives the mercury vapor pressure as a function of temperature.

B. RF Coupling and Plasma Initiation

The mercury plasma was generated and sustained by RF induction heating. A copper induction coil of 1/8" tubing was wrapped around the discharge tube with 8 turns and connected with transmission cable to an RF generator. Figure 9a shows the coil configuration. The RF source, a CVC AST-350 RF generator, operated at 13.56 MHz with a maximum output of 1 KW. The RF plasma in the discharge tube was started with a tesla coil after the generator had been turned on to a minimal power level.

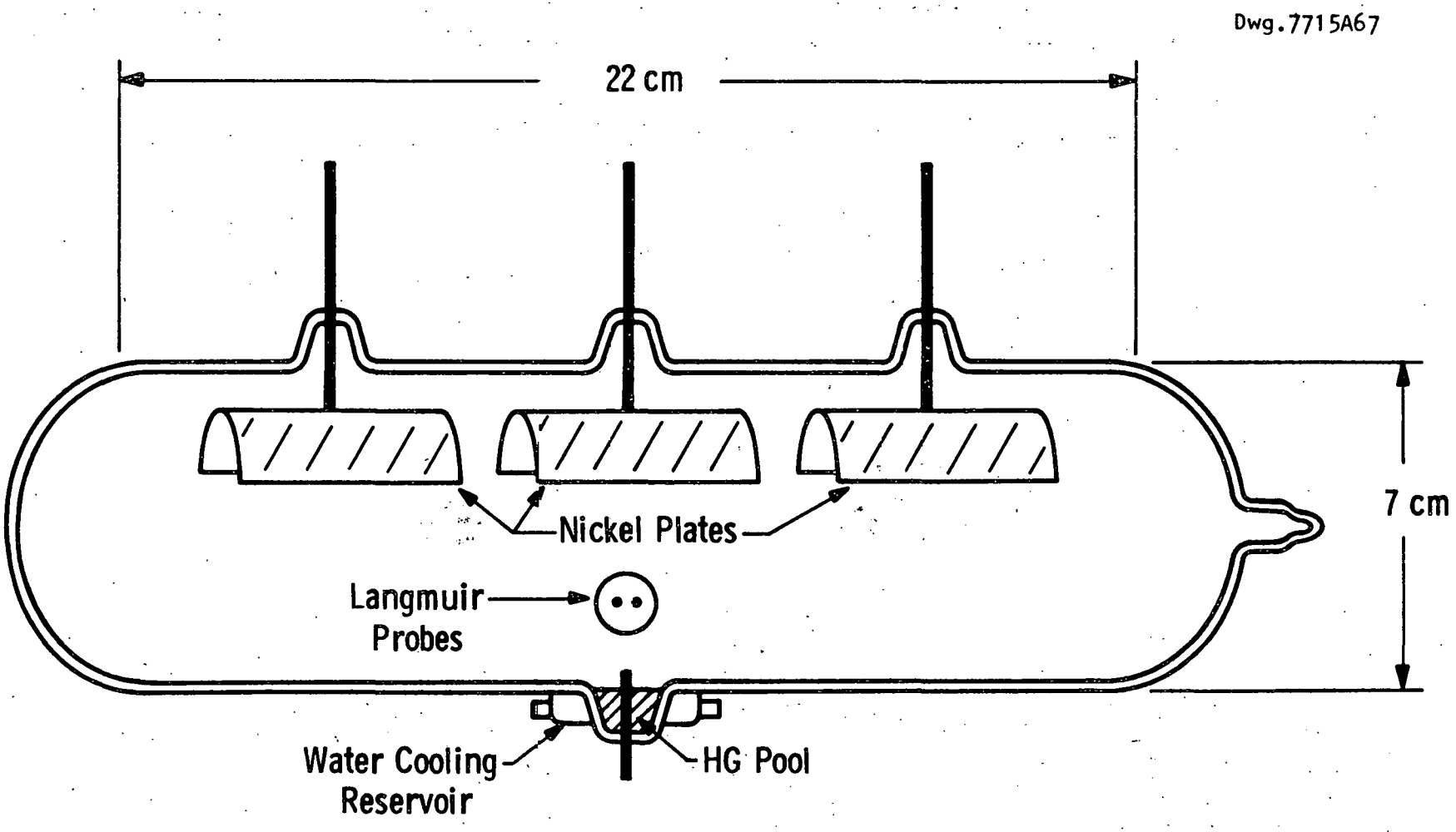

Figure 6. Unipolar Arc Discharge Tube.

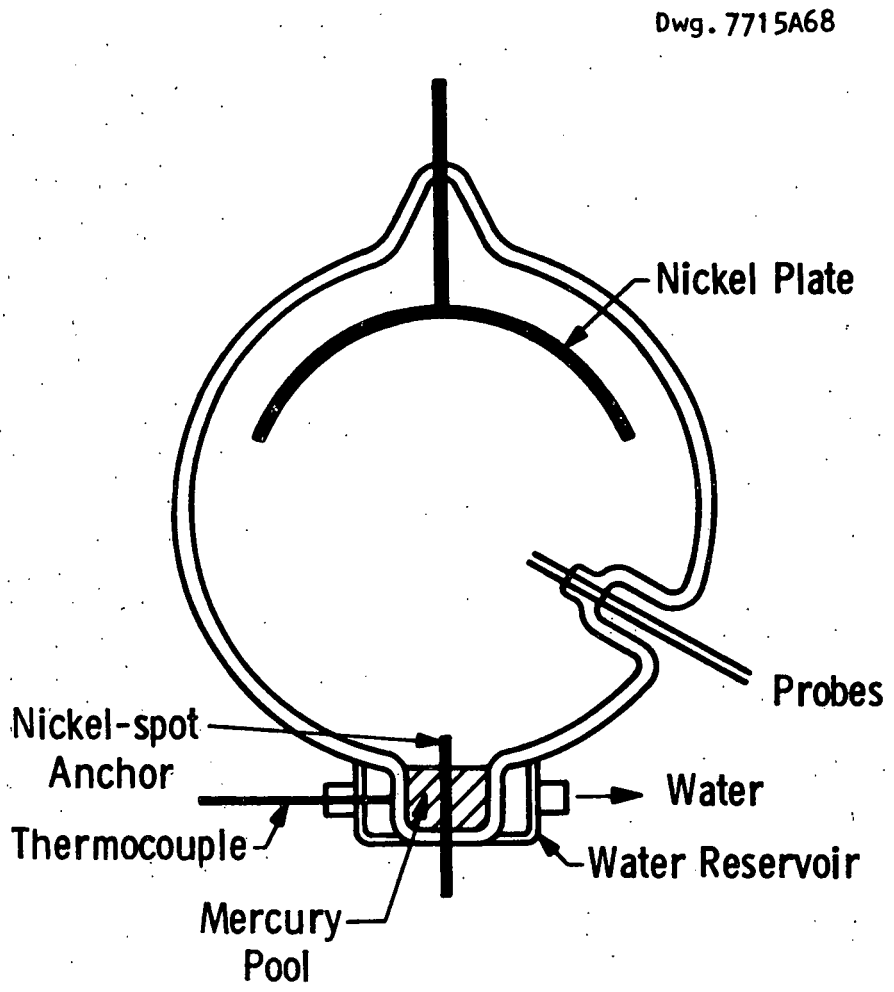

Figure 7. Cross-Sectional View of Discharge Tube.

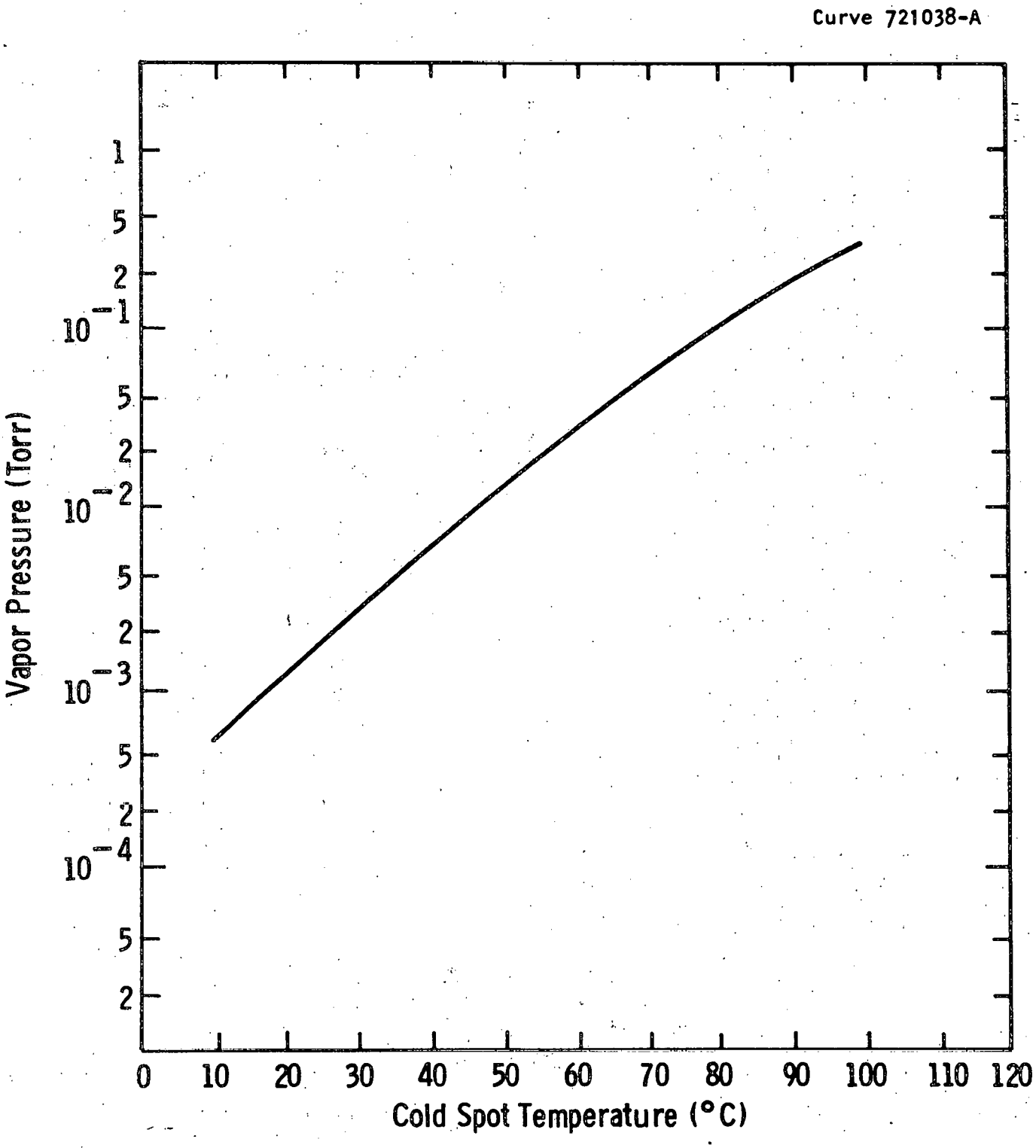

Figure 8. Mercury Vapor Pressure as a Function of Temperature (Ref. 23).

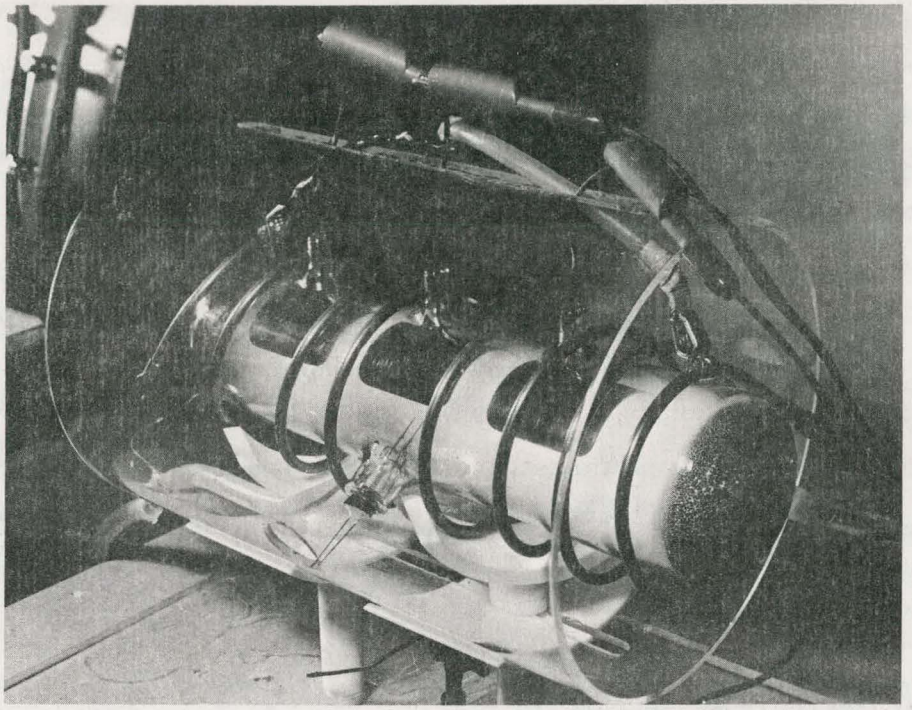

Figure 9A. Discharge Tube and RF Plasma.

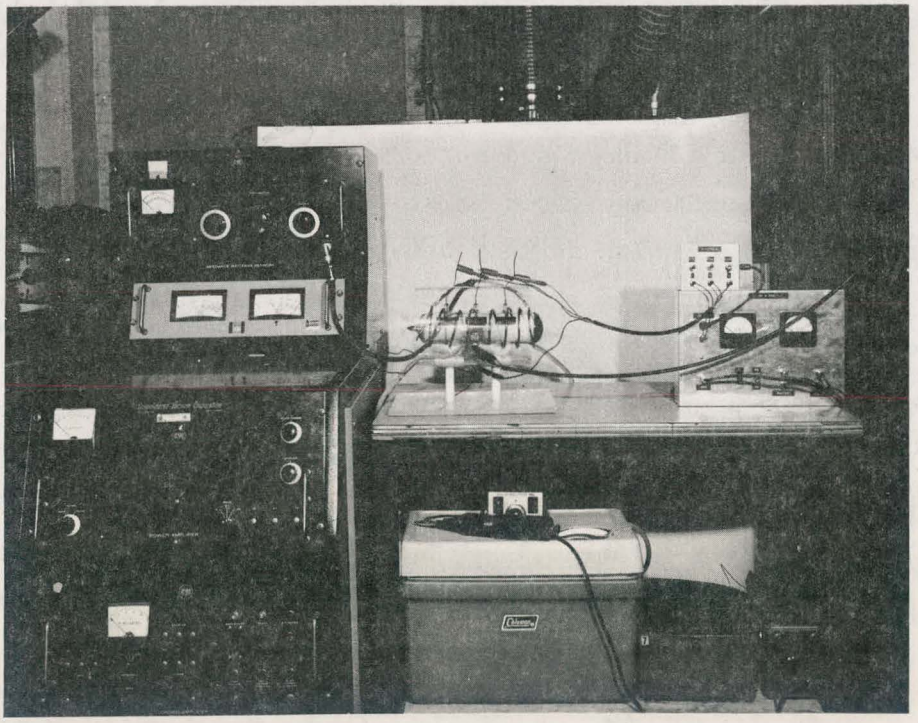

Figure 9B. Experimental Apparatus.

The RF power was then optimally coupled into the coil and the plasma by tuning the generator with its impedance matching network. Incident and reflected powers to the coil and plasma were monitored with Bird RF power meters. These power readings gave an indication of the power dissipated in the plasma since it could not be directly measured.

Optimal coupling was determined by first raising the RF power level until the monitored arc voltage reached the desired value. (The desired arc voltage will be discussed below.) At this voltage the impedance matching network was fine-tuned to give the same arc voltage at the lowest incident and reflected powers. Visual observation was also used to assure uniform brightness of the plasma throughout the discharge tube volume.

C. Switching Circuit and DC Arc Initiation

To initiate the arcing process and to stabilize the cathode spot on the nickel spot-anchor, a DC arc was struck between the nickel anode and mercury pool cathode with the voltage being applied by the 250 V DC power supply shown in the switching circuit of Figure 10. (Switch S2 was closed and switch S1 was open for DC arc initiation.) The arc voltage between the nickel anode and mercury pool cathode was monitored by a DC voltmeter. The DC arc could be struck with or without the RF on, but initiating the DC arc with an RF plasma present caused the RF plasma conditions to change enough to again require the RF impedance matching optimization process.

The 1.0 μF capacitor and 25 mH inductor in the switching circuit acted to filter the RF from the DC power supply. The DC ammeter and the oscilloscope across the .01Ω low inductance shunt monitored the arc current and its waveform in both the DC and unipolar arc modes. The cables to the discharge tube from the circuit were laid parallel to the axis of the tube to minimize the RF pickup. This cable was a twisted pair with a shield that was allowed to float. The grounding point was carefully selected for this circuit to minimize the RF pickup.

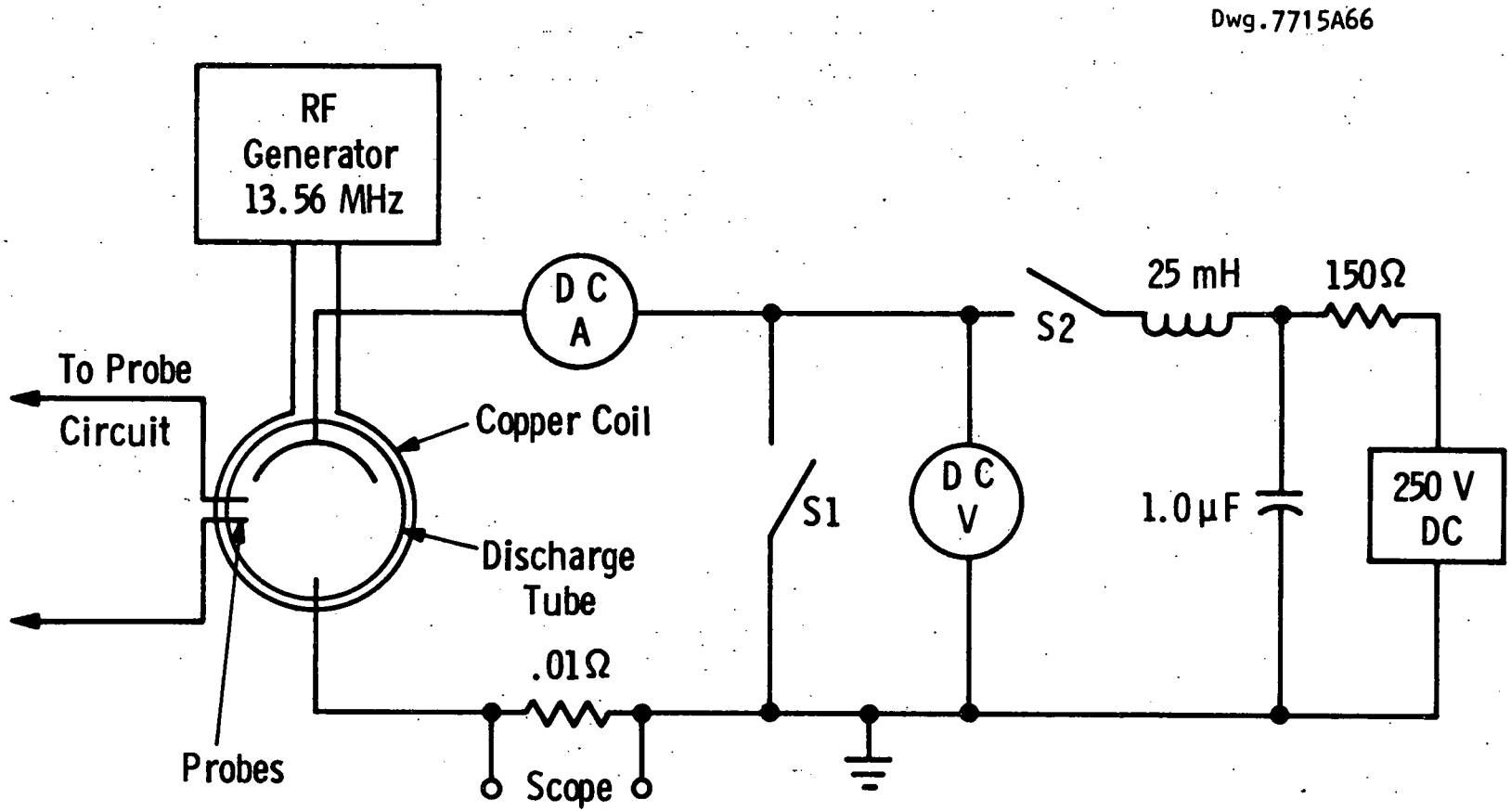

Figure 10. Switching Circuit.

The DC arc mode was defined for the switching circuit when the toggle switch S2 was closed and the mercury contact switch S1 was open. By closing S1 to connect the cathode and the nickel plates and then opening switch S2 to remove the DC supply, the system was put into the unipolar arc mode.

D. Unipolar Arc Mode

From the initial low power RF plasma (<100 W incident) and the DC arc, the arc voltage was monitored as the RF power was increased. The voltage was found to be a function of the RF power input so that it dropped from the 12.7 V of the DC arc to a negative value as the RF power was increased. The maximum negative voltage observed was -9 to -10 V. Below a voltage of -4 V with a DC arc current of 1 A or greater, the DC arc mode could be converted to the unipolar arc mode by the operation of S1 and S2. The DC ammeter and the oscilloscope continued to monitor a flow of the same polarity current throughout the switching process.

In Figures 11a and 11b the unipolar arc mode configuration for this experiment is compared to that for the fusion reactor first wall in contact with a plasma. The first figure in 11a is a view of the discharge tube's cross section. The second is a rearrangement of that geometry for a comparison with Figure 11b. In the case of the first wall, the cathode material is the same as that of the electron collecting surface. ("Electron collecting surface" is used for the unipolar arc mode rather than "anode" as will be discussed in Section V.) In this experiment the cathode is a mercury pool while the electron collecting surface is a nickel plate.

E. Probe Characteristics

Probe characteristics of the RF plasma alone, the DC arc plasma with and without RF, and the unipolar arc plasma were taken with the aid of the circuit shown in Figure 12. By adjusting the 5 kΩ potentiometer, the differential probe voltage V was varied from a minimum of -9 V to a maximum of 9 V or from a minimum of -6 V to a maximum of 6 V depending upon the particular run. The current drawn through the probes was monitored by measuring the voltage drop across the 1.8 kΩ resistor and plotted as a function of the differential probe voltage on an X-Y recorder.

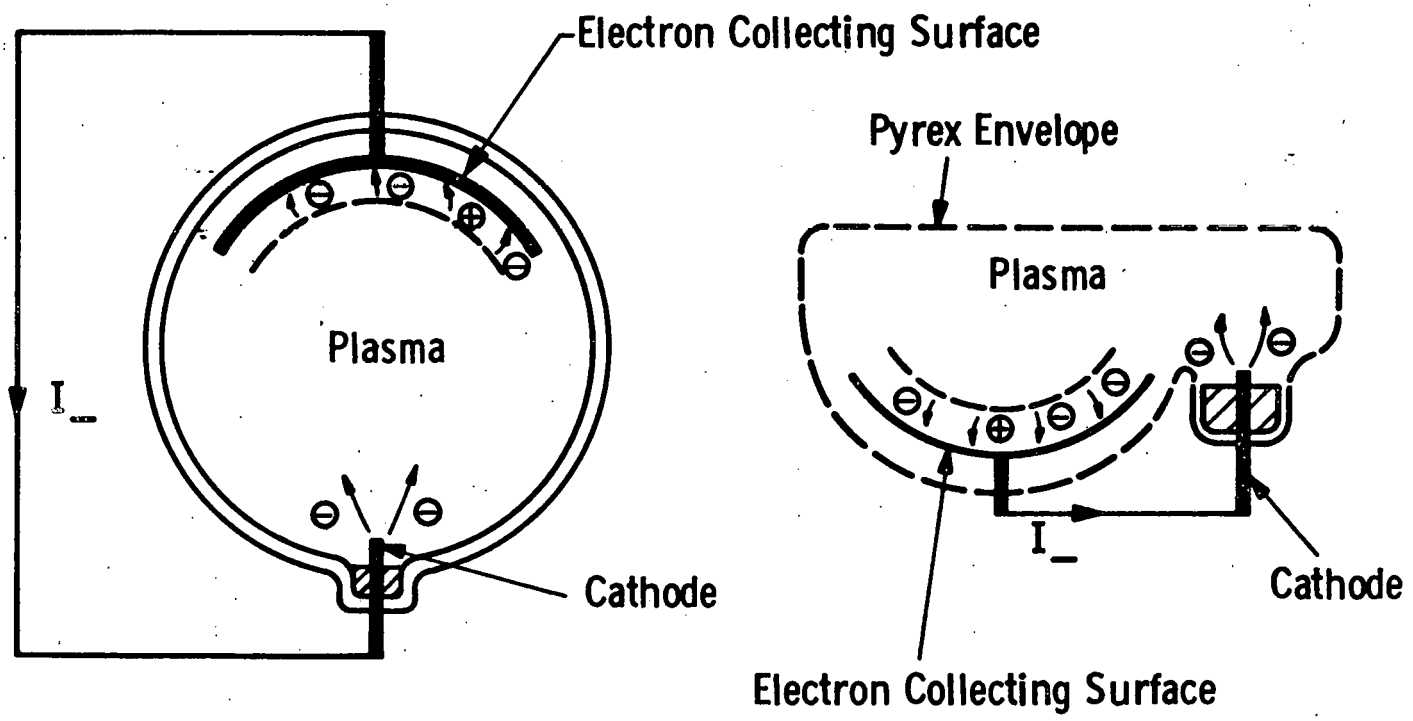

Figure 11a. Configuration of the Unipolar Arc Mode in the Mercury Discharge Tube.

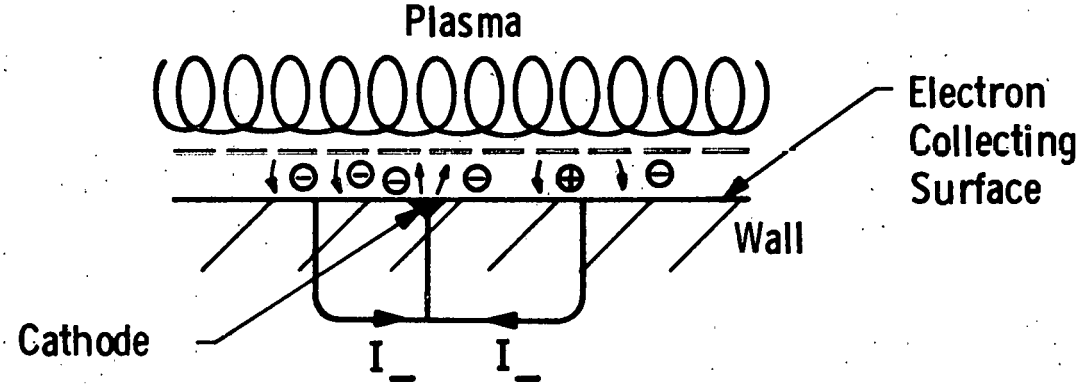

Figure 11b. Configuration of the Unipolar Arc Mode for a Fusion Reactor.

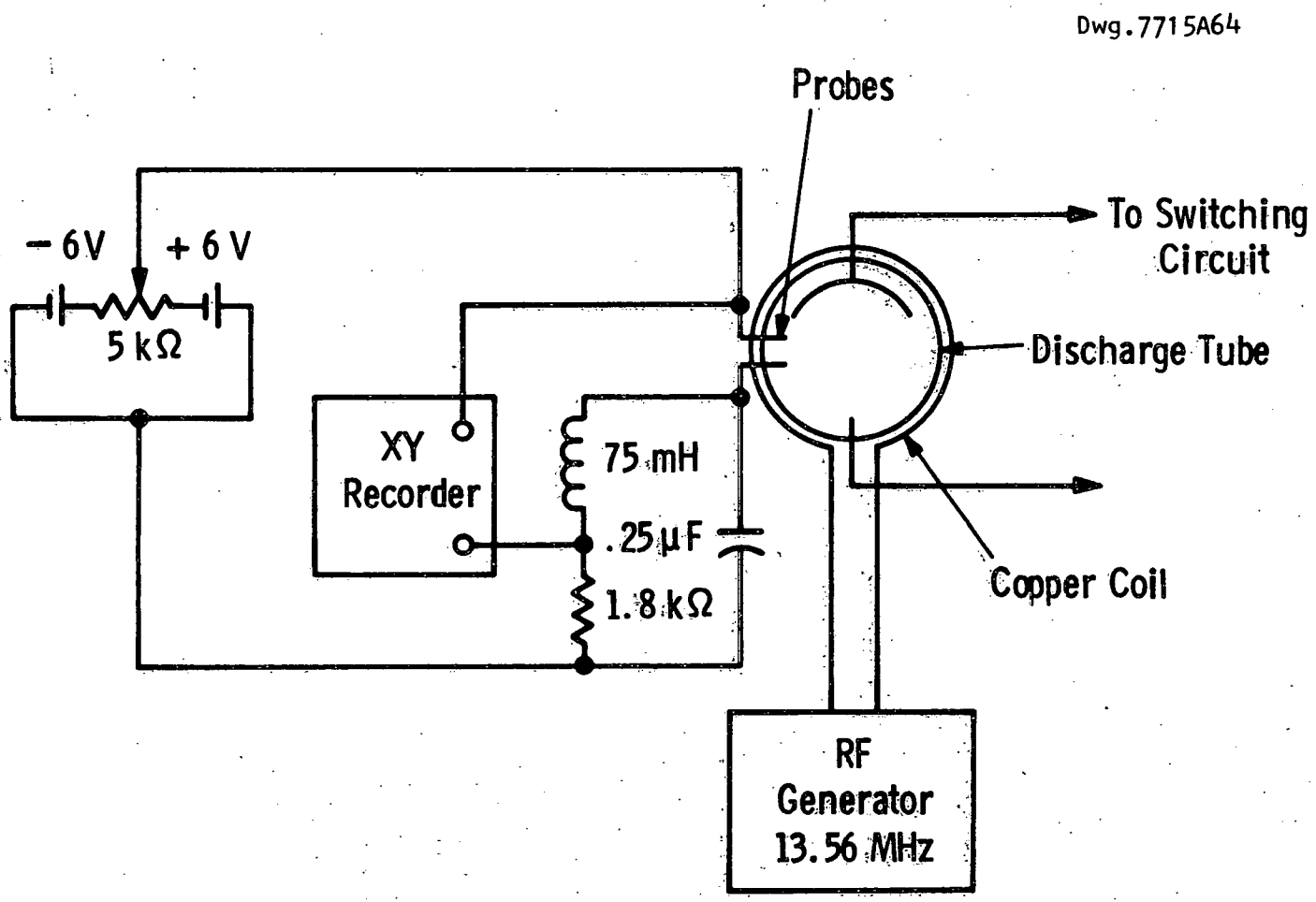

Figure 12. Probe Circuit.

The leads for the probes were a twisted pair of wires with a floating shield. This cable was brought from the discharge tube along a line parallel to that of the tube's axis. This was necessary to reduce the RF pickup. If the amount of incident RF power was greater than 600 W and the reflected RF power was greater than 55 W, the probe data deviated from the desired characteristic shown in Figure 5. This will be discussed in further detail in Section V.

F. Data Collection

With the experimental apparatus as described above, studies were conducted by monitoring:

1) the arc current and its waveforms
2) the arc voltage before switching
3) the probe characteristics
4) the RF power settings
5) the mercury pool cathode temperature at the glass wall.

IV) RESULTS

A. General Observations

Initiation of the DC arc was most easily accomplished by applying 250 V across the anode and cathode with a small amount of RF power sustaining a plasma. As the DC voltage was turned up from 0 to 250 V, prior to the arc initiation, the bright RF plasma region could be seen to draw away from the cathode area. As the RF power was then increased the bright plasma dropped slowly down towards the cathode until it seemed to touch the mercury pool. At this instant the DC arc would be initiated and the cathode spot would run around the edge of the pool. Eventually the cathode spot would settle onto the nickel spot-anchor as a bright ring circling at the interface of the mercury and the nickel spot-anchor. The arc initiation changed the plasma parameters so that both the incident and reflected RF powers decreased about 10 to 20% and the plasma intensity changed. As described the impedance matching network was fine-tuned at this point. The RF incident and reflected wattages ran at a minimum of 310 W and 32 W respectively for unipolar arcs. But in most cases it was necessary to use more than 600 incident watts due to the specific impedance matching conditions required. The ratio of incident to reflected power was approximately 10 for both DC and unipolar arc modes.

Increasing the RF with the DC arc caused 1) the arc voltage to drop from 12.7 V and 2) the plasma to become more intense throughout the discharge volume. Finally as the voltage was pushed below -4 V the switching of S1 and S2 could be done while the arc's cathode spot remained visible at all times. In the unipolar arc mode the DC supply was completely removed from the circuit.

The switching at -4 V in many cases caused the cathode spot to move off the anchor and eventually extinguish. This was also noted

as the monitored current dropped to zero. In some cases the cathode spot would try to re-establish itself, but could not anchor stably again. Switching at ∿-8 V resulted in a more stable unipolar arc. Data on the unipolar arc current, its waveforms and probes could not be taken unless the cathode spot was firmly anchored on the nickel spot-anchor.

The unipolar arcs could last up to 20 minutes with most of them lasting less than 5 minutes. After the arcs extinguished it was not possible to initiate them again for several hours as the system cooled. The cathode wall temperature was maintained at ∿20° C.

Three arc tubes of the same design were used for collecting these data. After running the discharge tube under high RF power input, a permanent, silvery coating, presumed to be mercury, began to adhere to the walls of the tube. This coating prevented a sufficient amount of RF from being pumped into the plasma as was indicated by the inability to drop the arc voltage below -1 to -2 V before switching. Indeed with the coating present the percentage of RF radiated was noticeably higher at a particular incident power and optimal impedance matching setting since all metal surfaces in the near vicinity would become slightly "hot" through skin effect heating. As the coating became heavier a greater amount of RF power was needed to create unipolar arcs.

B. Unipolar Arc Data

i) Unipolar Arc Current Waveforms

Waveforms of the unipolar arc current typically appeared as in Figure 13b. The traces show 1) the RF modulation at 13.56 MHz and 2) the DC displacement from ground as indicated. The portion of the RF amplitude attributed to pickup was minimized by use of the twisted-pair cable, the line along which the cable was laid with respect to the discharge tube axis, and the choice of the grounding point in the switching circuit. The DC current values from the oscilloscope waveforms agreed with those shown by the DC ammeter in the switching circuit. (Figure 13a, for comparison, is that of a 1.35 A DC arc in a low power RF plasma.)

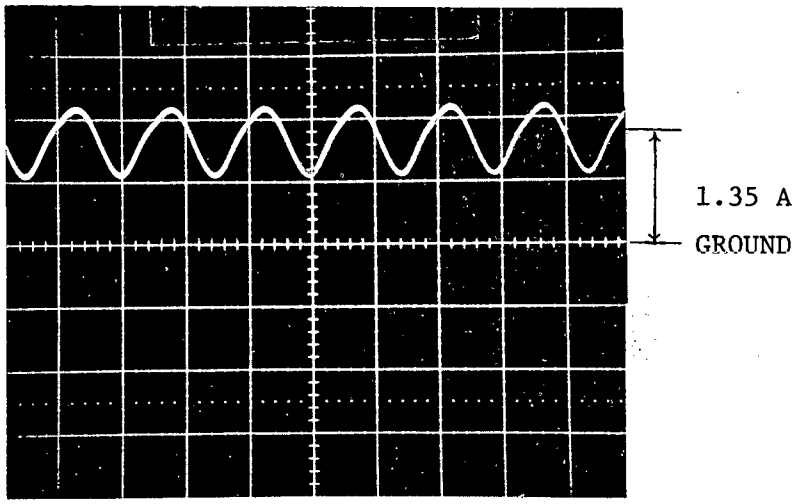

Figure 13a. 1.35 A DC Arc in a Low Power RF Plasma (RF Incident Power ∿ 95 W).

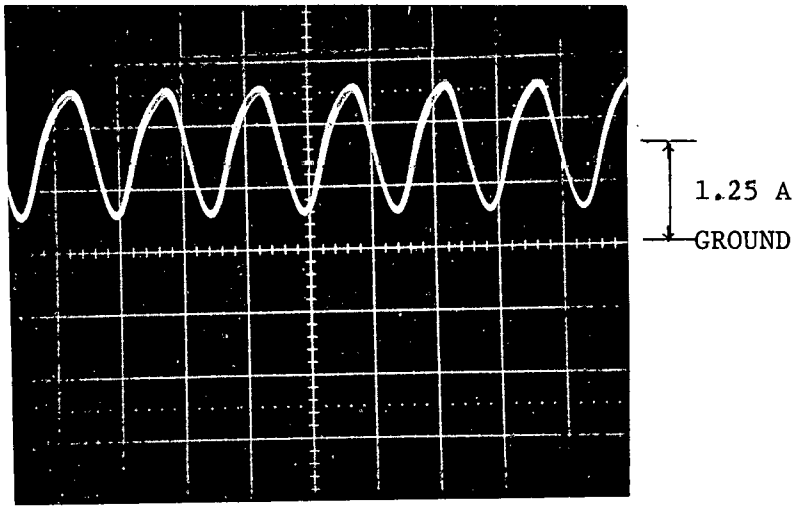

Figure 13b. 1.25 A Unipolar Arc (RF Incident Power ∿ 330 W). Scales for both photographs { 1 A/cm and 50 nsec/cm }.

The current waveforms were observed from the point at which the DC arc was initiated, with a minimal amount of RF power input, through the switching operation to the unipolar arc mode. The sinusoidal shape and frequency of the waveforms did not change. The sinusoidal amplitude however did increase with the RF power increase. The sinusoidal waveform presumably was due to instrumentation pickup and not actual current measurements. At switching the current was observed to increase from the 1 to 1.35 A of the DC arc to as much as 2.1 A for the unipolar arc. The amount by which the current increased was determined by the negative voltage level prior to switching. The 2 A current reading corresponded to an arc voltage of -8V or so.

ii) Variation of Unipolar Arc Current with RF Power Input

Once the system was in the unipolar arc mode at a given current, the probe characteristics were taken to obtain T_e and n_e. Figure 14a shows a typical probe characteristic of a unipolar arc plasma at 1.2 A with T = 2.02 eV and $n_e = 2.4 \times 10^{11}$ cm^{-3}. (A DC arc plasma typically gave a T_e of .5 eV and an $n_e = 1 \times 10^{10}$ cm^{-3}.) The unipolar arc current was varied by increasing or decreasing the RF power input and the probe characteristics recorded at each current level. Tables 1 and 2 (page 40) give the T_e and n_e values for the measured unipolar arc currents I_c at 1.5, 1.75, and 2.1 A obtained as the RF power was varied. Figure 14b shows the probe characteristic for the 1.75 A reading. For a greater range of differential probe voltages the saturation currents oscillated above and below the saturation values.

iii) Variation of the Unipolar Arc Current with the Metal Plate Surface Area

The three nickel plates were always used in the initiation of the arcs. After stabilization of the unipolar arc any one electrode could be removed. The arc current change was noted. With three plates and a switching voltage of -8 V the unipolar arc current registered 2.1 A. Removing the center plate caused the current to drop to 1.6 A. Switching to a single electrode caused the unipolar arc to extinguish. Unfortunately the probe characteristics could not simultaneously be taken due to the instability of the arc. The arc anchored long enough to record the external circuit currents, but not long enough to take the probe characteristics.

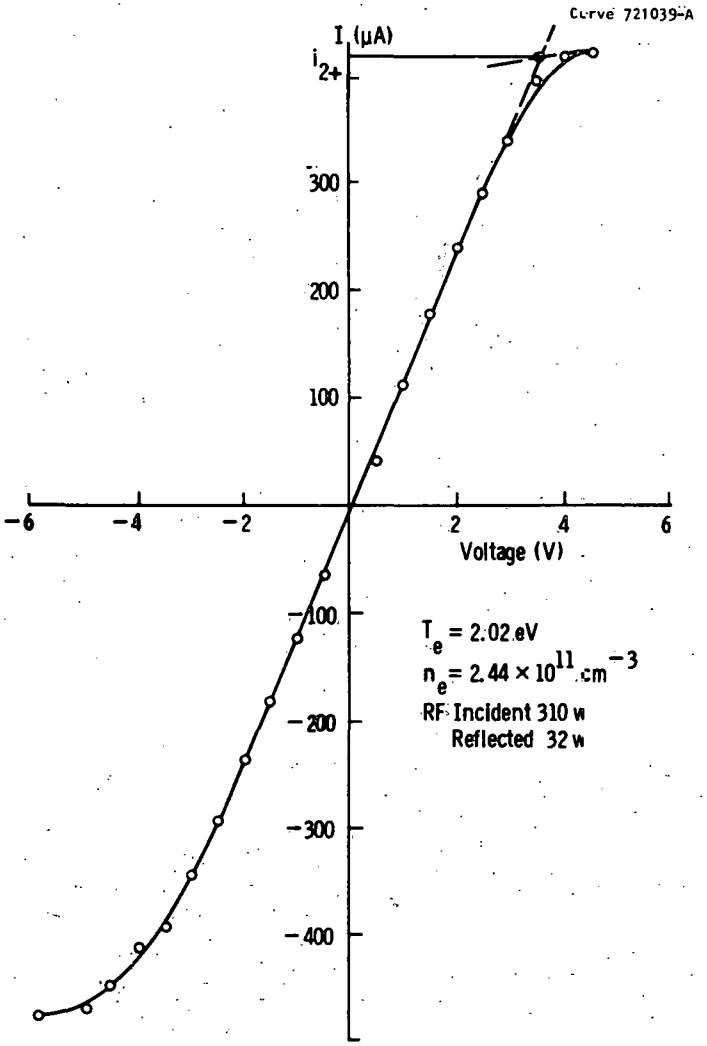

Figure 14a. Probe Characteristic fcr 1.2 A Unipolar Arc.

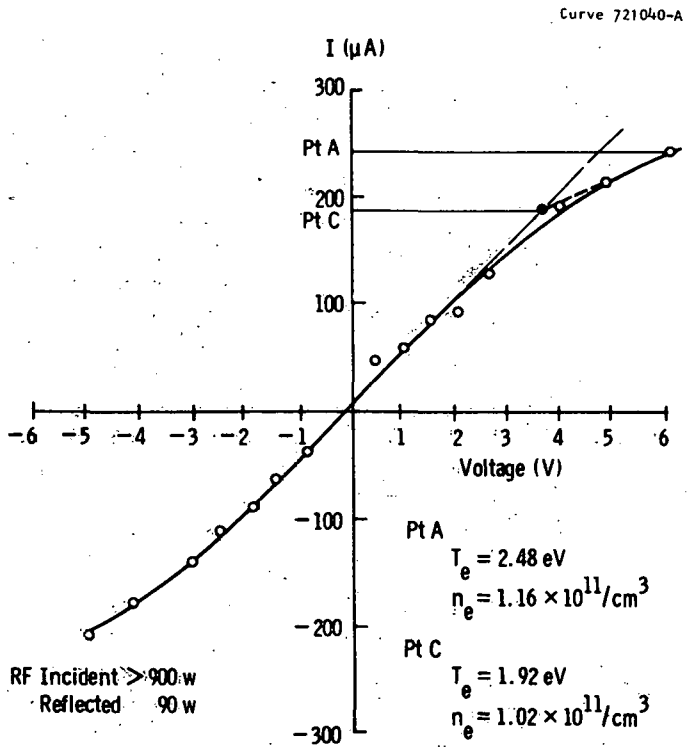

Figure 14B. Probe Characteristic for 1.75 A Unipolar Arc.

V. DISCUSSION

A. Unipolar Arcs

i) The Sheath Voltage V_s

The transition from the DC arc mode to the unipolar arc mode was characterized by a decreasing arc voltage with increasing RF power input. This decrease in voltage signified that the plasma conditions were changing to increase the plasma density and/or the electron temperature. T_e was typically observed to increase from $\sim$.5 eV for the DC arc to approximately 2 eV for the unipolar arcs with n_e increasing from $\sim 1 \times 10^{10}$ cm^{-3} to $\sim 1 \times 10^{11}$ cm^{-3}. The increase in n_e from the DC to the unipolar arc mode may have been due to

1) an increase in the neutral density,

or

2) an increase in the ionization efficiency

with RF heating. The probe characteristic monitored in the transition region, as the voltage dropped from 12.7 V for the DC arc to negative voltages for the unipolar arc, was inconclusive as to the functional dependence of the T_e and n_e changes. This dependence, however, is of considerable interest to the basic understanding of the transition process.

By substituting these measured T_e values for the unipolar arc plasma into Eq. 21

$$V_s = \frac{kT_e}{2e} \ln\left(\frac{m_i}{2\pi m_e}\right) \qquad (21)$$

the sheath potential for the unipolar arc mode was found to be $\sim$11 V. Given then that the cathode fall V_c is 9 V, this value of V_s meets the criterion for unipolar arcs that

$$V_s \geq V_c \qquad (26)$$

Figure 15 shows a schematic representation of the plasma as the potential V_s builds up. V_s opposes V_c which accounts for the decrease in the observed voltage. In the build up of V_s the anode or positive drawing point for the electrons is pushed down into the plasma away from the nickel surfaces by several Debye lengths in accordance with sheath theory. For our plasma conditions a Debye length was approximately 3×10^{-3} cm^{-3}. This shift of the anode from the nickel plates for the DC arc into the plasma for the unipolar arc is a critical concept for the unipolar arc theory. In the unipolar arc mode the nickel plates still serve to collect the electrons as in the DC arc mode but they no longer act as the complete anode. The electrons are collected by the nickel plates which are directly connected to the cathode or electron emitting surface. The unipolar arc mode of operation, therefore, allows a single plate to collect and emit electrons in the fusion first wall configuration.

ii) Negative Arc Voltages

As described the switching procedure from DC to unipolar arc modes could be accomplished below -4 V. The various potential drops in the system:

1) that across the plasma $I_c R_p$ (1 or 2 V)

plus

2) that for the cathode fall V_c

would require a sheath potential V_s of approximately 11 to 12 V to sustain a unipolar arc. An arc voltage reading close to zero prior to switching would thus be expected given that the DC arc voltage without RF registered 12.7 V.

The negative voltage readings can be explained, however, by the following. The DC power supply was a constant current source and was set for arc currents of 1.35 A or less. Upon switching to the unipolar arc mode the current was observed to increase to as much as 2.1 A. In order to suppress the current to 1.35 A, as dictated by the DC supply before switching, an additional negative voltage was needed at the sheath to repel all but 1.35 A of the electron current. This additional voltage

Dwg.7715A63

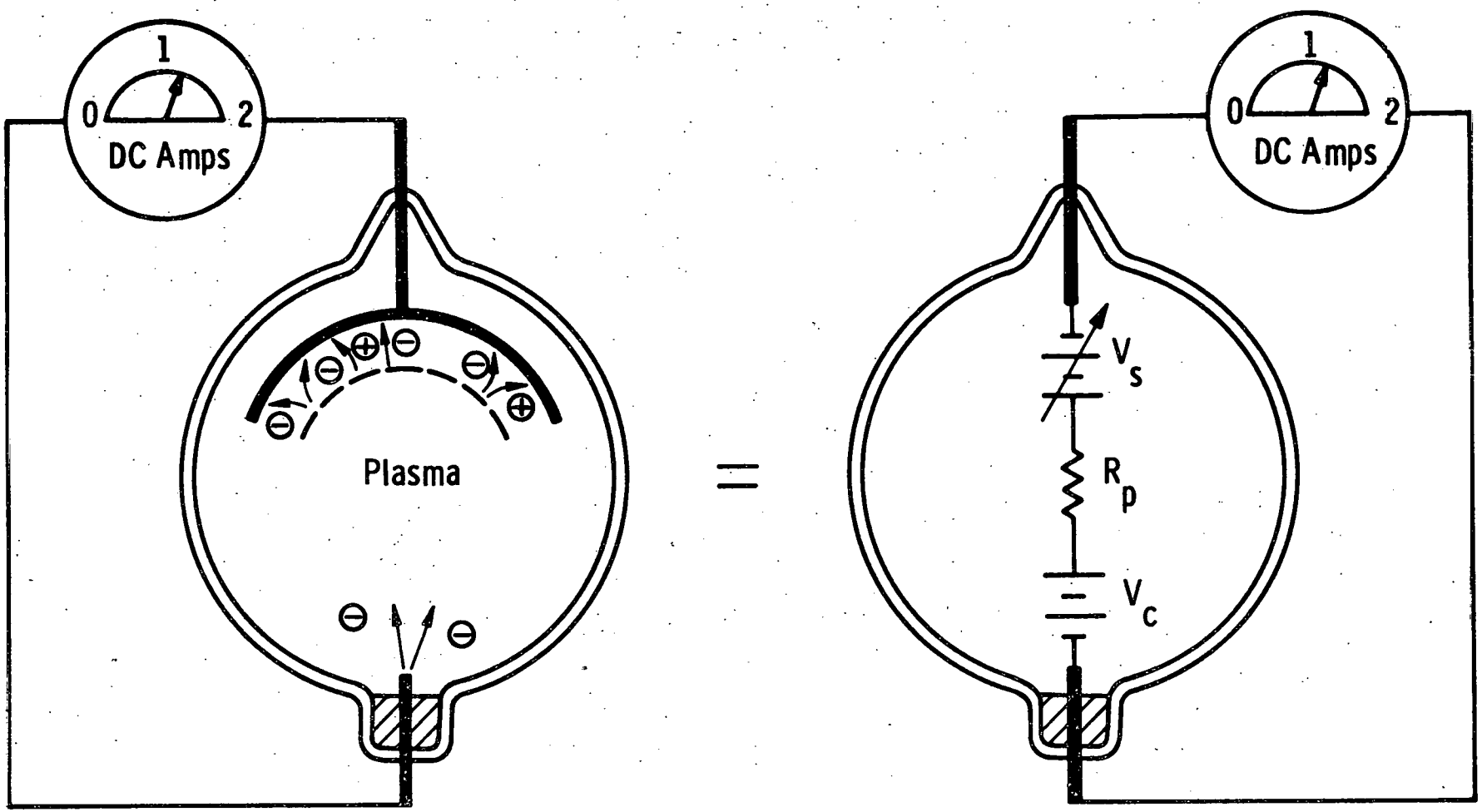

Figure 15. Schematic of Unipolar Arc Driving Mechanism.

plus the 11 V required to sustain the potential drops across the plasma and at the cathode, by the convention shown in Figure 15, opposed the DC arc voltage. Thus negative voltage readings resulted. Once the DC supply was removed the sheath voltage presumably returned to the ∿11 V level as indicated by the T_e values of ∿2 eV observed for unipolar arcs.

iii) Saturation Ion Currents

Some difficulty was encountered in the determination of the saturation ion currents i_{1+} and i_{2+} which go into the calculation of T_e and n_e (Eq. 40). In Figure 14a the saturation regions level off in such a manner that the current values at the intersection of the y axis (Pt. C) are within 10% of the current values at the maximum positive and negative differential probe voltages. The incident RF was 310 W and the reflected was 32 W for this particular probe characteristic. When a large amount of RF power (>600 W incident and >55 W reflected) had to be used to establish stable unipolar arcs, the current did not completely saturate. As in Figure 14b, for example, the currents are seen to reach regions at the high and low voltages where the rate of rise is not as steep as that of the central voltage region but it is still significant. The incident RF was >800 W and the reflected was 80 W. The value of the ion saturation current i_{2+} at Pt. C is 30% less than that at Pt. A. These various points for evaluating the ion saturation current were discussed in Section II. The resulting T_e and n_e values are

Pt. A $\quad T_e = 2.48$ eV

$\quad n_e = 1.16 \times 10^{11}$ cm^{-3}

Pt. C $\quad T_e = 1.92$ eV

$\quad n_e = 1.02 \times 10^{11}$ cm^{-3}

for Figure 14b.

As previously described a non-Maxwellian temperature distribution with several temperature components may account for the effects in the saturation regions. Single probe measurements should resolve this question concerning the temperature components. Similar procedures were used in determining i_{1+}.

iv) Unipolar Arc Current

Using Eq. 25 to calculate the unipolar arc current I_c, a comparison with the measured I_c was made. The T_e and n_e values, computed from the ion saturation currents taken at the asymptote intersection and the maximum ion current, were used in this calculation. Table 1 and Table 2 summarize this information for the unipolar arc currents of 1.5, 1.75, and 2.1 A monitored as the RF power was varied. In Table 1 the results were calculated from the ion saturation currents taken at the asymptote intersections (Pt. C). The values in Table 2 were calculated from the maximum ion saturation current (Pt. A). The calculated currents I_c were found to be quite sensitive to the electron temperature due to the exponential dependence of Eq. 25 on T_e. A 25% change in T_e brought about a factor of 10 difference in the calculated currents.

Specifically, the calculated values of I_c in Table 1 are a factor of $\sim$10 below the monitored current, and they do not increase with the RF power. In comparison, the calculated values of Table 2 are in close agreement with the measured values. Table 2 shows that T_e remained fairly constant with increasing RF power while n_e changed sufficiently to bring about the observed change in I_c. In other words, I_c is proportional to the ion saturation current. Figure 16 shows this relationship between I_c and I_{SAT}. (See Eqs. 25, 29, and 30.)

Table 1

I_c (measured)	RF (reflected)	T_e (eV)	n_e ($\times 10^{11}$ cm^{-3})	V_s (V)	I_c (calculated)
1.5 A	75 W	1.92	1.02	10.5	.29 A
1.75 A	80 W	1.76	1.43	9.7	.15 A
2.1 A	90 W	2.05	1.68	11.3	.81 A

Table 2

I_c (measured)	RF (reflected)	T_e (eV)	n_e ($\times 10^{11}$ cm^{-3})	V_s (V)	I_c (calculated)
1.5 A	75 W	2.48	1.16	13.6	1.66 A
1.75 A	80 W	2.40	1.67	13.2	2.03 A
2.1 A	90 W	2.54	1.87	13.9	2.99 A

Tables 1 and 2 give the plasma parameters and the arc currents as a function of RF power. Both tables use the same data but different interpretations of that data.

The calculated current for the probe characteristic of Figure 14a was 1.05 A while the measured value was 1.2 A. In general, when the ion saturation regions of the probe characteristics were relatively flat 1) the Pt. A and Pt. C ion saturation discrepancy was obviously less and 2) the calculated currents were closer to the monitored currents. As described above, the slope of the ion saturation region seemed to increase with the RF power input. This may have been due to a change in the electron energy distribution so that several temperature components were present. It should be noted that all electron temperature of Tables 1 and 2 are sufficient to give a sheath potential greater than the cathode fall.

v) Surface Area Effects

Equation 25 also shows the arc current to be directly proportional to the electron collecting surface area A. This relationship was studied by using several combinations of the three nickel plates. The unipolar arcs were initiated with three plates at an arc current of 2.1 A. By removing the center plate (Figure 6) and allowing it to float, the current was made to drop to 1.6 A. Switching to one plate caused the arc to die.

The drop in current from 2.1 A was expected although a proportional decrease with the plate area drop of 2/3 would take I_c to 1.4 A. The plasma changed in intensity at the removal of the center plate indicating that the plasma parameters had changed in such a way to instead support a 1.6 A current. Without probe characteristics the nature of this change with T_e, n_e, or both is unknown.

Several attempts to support the unipolar arc with one plate failed. Presumably the 28 cm^2 of the single plate collected an insufficient number of electrons to maintain the 1 A or so needed to keep the cathode spot on the mercury pool cathode alive.[24]

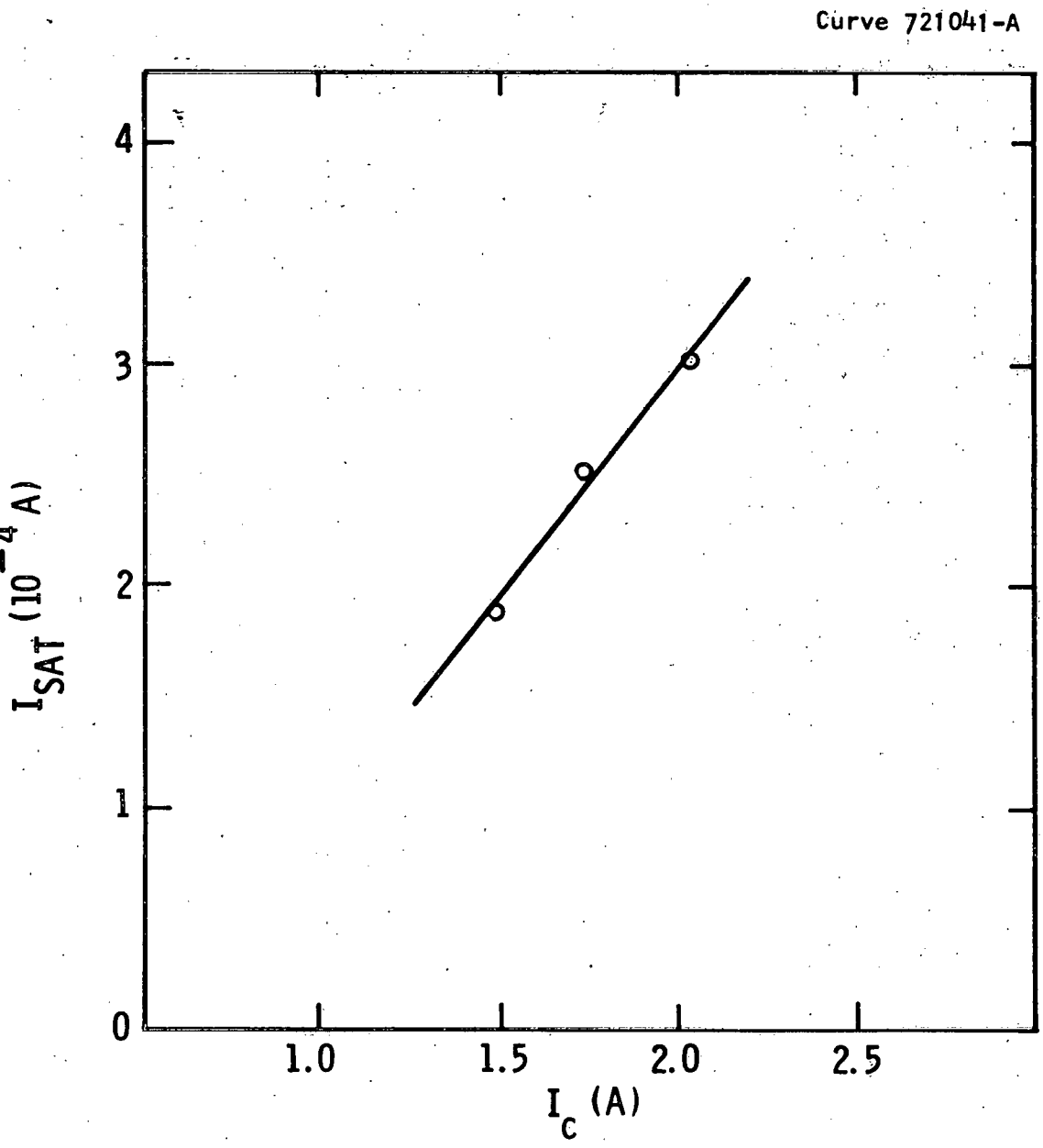

Figure 16. Ion Saturation Current as a Function of Unipolar Arc Current.

B. Alternative Arc Driving Mechanisms

i) Full-Wave Rectification[25]

The inductive RF heating mechanism, which sets up electric fields on the surface of the plasma, was considered as an alternative explanation for the observed results. The surface electric fields could connect the anode and cathode as is schematically shown in Figure 17, and provide the path whereby the current would flow between the electrodes. Since the fields change only their aximuthal direction every 1/2 cycle, the mercury pool could remain the cathode at all times. The system would thus operate in a pulsed DC mode while sustaining the cathode spot. The current waveform would indicate full-wave rectification, but this was not observed, (Figure 13).

ii) Half-Wave Rectification[26]

Another RF mechanism for sustaining the observed arcs could result from capacitive coupling of the stray RF to the nickel plates. The induced voltages at the 13.56 MHz would cause current to flow only on the positive half-cycle. In this half-cycle the plates would act as the anode and the mercury pool as the cathode. In the negative half-cycle, current would not flow since the nickel plates could not act as the cathode at the 1 A current. The expected current waveforms would be half-wave rectified, but this was not observed, (Figure 13).

RF rectification effects were therefore ruled out as possible alternative mechanisms for sustaining the observed arcs.

Dwg.7715A60

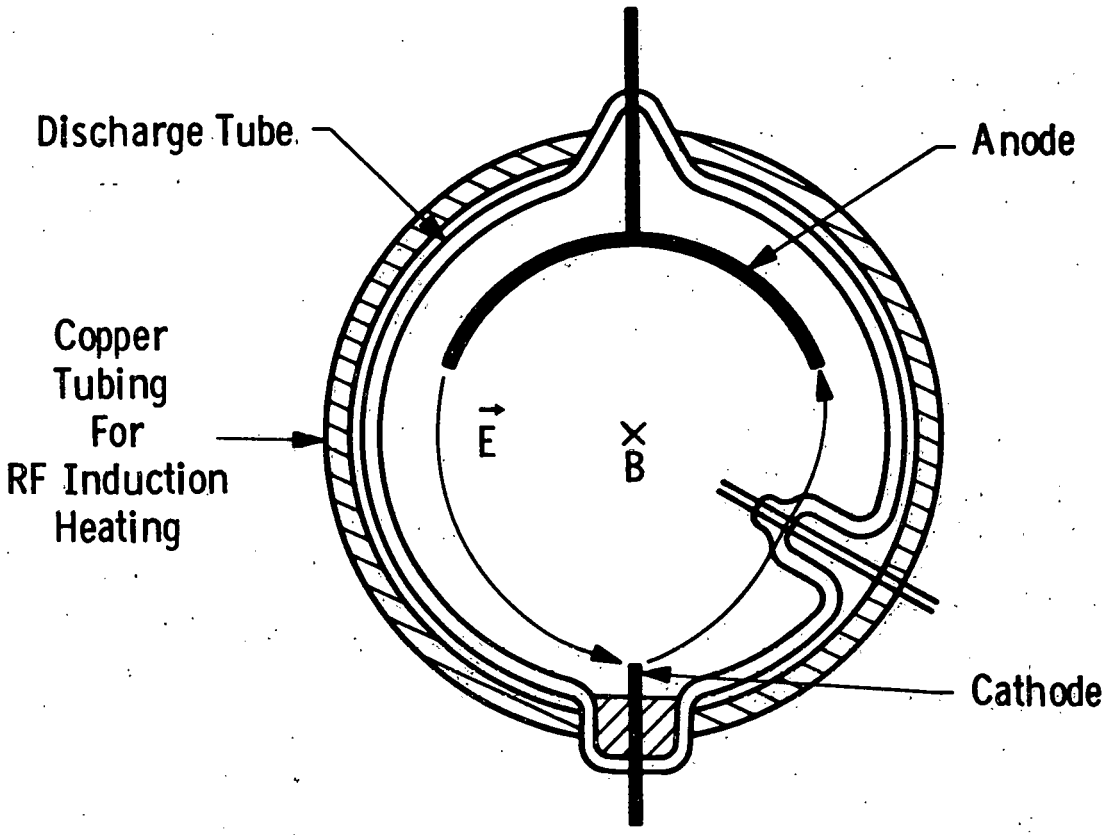

Figure 17a. Electric Field Configuration Set Up by the RF Fields.

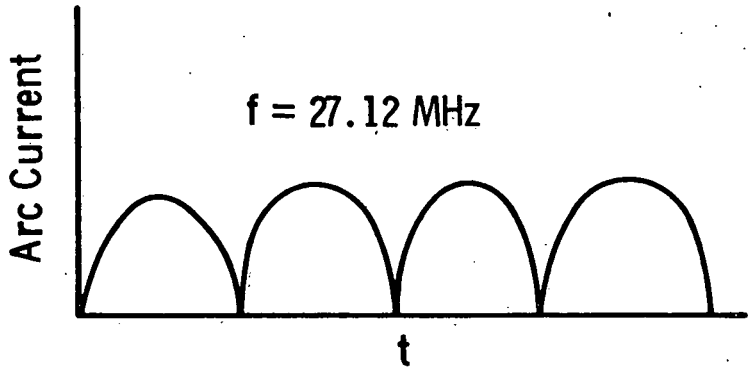

Figure 17b. Full-wave Rectification: Expected Current Waveform for High Frequency Rectification.

VI. CONCLUSIONS AND RECOMMENDATIONS

The characteristics of the unipolar arcs, created in a low pressure mercury discharge inductively heated with RF, were found to be consistent with the sheath theory. The transition from a bipolar DC arc to a unipolar arc was accomplished through increasing the RF power input to the plasma. The arc current and decreasing arc voltage monitored throughout this process were consistent with the model of changing plasma conditions needed to build the sheath. A more in-depth study of the transition and its effects on the electron temperature T_e and the electron number density n_e would be of great interest.

The electron number densities n_e and the electron temperatures T_e measured with the floating double-probes for the unipolar arc plasma were sufficient to sustain a sheath potential V_s greater than the cathode fall V_c of a mercury pool cathode. The unipolar arc current I_c was found to be proportional to the metal surface area exposed to the plasma. This was predicted by the theory in Eq. 25. The monitored unipolar arc current was found to increase with increasing RF power input. The arc currents, calculated from the measured T_e and n_e values, were found to be strongly dependent upon the electron temperatures and the ion saturation currents which changed with the RF power. Since the probe characteristics suggested that the electron energy distribution deviated from a Maxwellian, had several temperature components, single probe measurements should be conducted to provide more specific information on the temperature components.

Alternative mechanisms for sustaining the observed arcs through high frequency rectification were considered. The recorded current waveforms ruled out such arc driving mechanisms.

Future studies with various cathode materials, different gases, alternative plasma heating mechanisms, and single probes could additionally support the findings of this experiment in the light of the unipolar arc sheath theory. Extending the study to experiments creating plasma

conditions similar to those in fusion reactors are specifically needed since it is not possible to make direct extrapolation from the findings reported here to the fusion case. Information leading to the understanding of the initiation process, the sustaining plasma conditions, and the causes of the unipolar arc extinction are of great relevance to fusion research.

REFERENCES

1. D. R. Porto and C. W. Kimblin, Visit to Arcing Phenomena in Fusion Devices Workshop, W R&D Trip Report No. 79-C72-1.

2. D.H.J. Goodall and G. M. McCracken, "Arcing and Surface Damage in DITE", CLM-R167, Culham Laboratory (Nov. 1977).

3. P. J. Harbour and M.F.A. Harrison, "The Influence of Electron Emission of the Divertor Target of a Tokamak Fusion Reactor", CLM-P528, Culham Laboratory (April 1978).

4. D.H.J. Goodall, T. W. Conlon, C. Sofield, and G. M. McCracken, "Investigations of Arcing in the DITE Tokamak", J. of Nucl. Mat. 76 and 77 (1978) pp. 492-498.

5. G. M. McCracken and P. E. Stott, "Plasma-Surface Interactions in Tokamaks", Nucl. Fus. 19 (1979) pp. 889-981.

6. G. M. McCracken and D.H.J. Goodall", The Role of Arcing in Producing Metal Impurities in Tokamaks", Nucl. Fus. 18 (1978) pp. 537-543.

7. S. A. Cohen, H. F. Dylla, S. M. Rossnagel, S. T. Picraux, J. A. Borders, and C. W. Nagee, "Long-Term Changes in the Surface Conditions of PLT", J. of Nucl. Mat. 76 and 77 (1978) pp. 459-471.

8. L. Oren, R. J. Taylor, and F. Schwirzke, "Phenomenology of Metal Influx in Macrotor", J. of Nucl. Mat. 76 and 77 (1978) pp. 412-417.

9. G. Staudenmaier, P. Staib, and F. Venus, "Impurity Fluxes in the Scrape Off Layer of TFR 400 and TFR 600", J. of Nucl. Mat. 76 and 77 (1978) pp. 445-451.

10. A. E. Robson and P. C. Thonemann, "An Arc Maintained on An Isolated Metal Plate Exposed to a Plasma", Proc. Phys. Soc. 73 (1959) pp. 508-512.

11. J. E. Allen and P. C. Thonemann, "Current Limitation in the Low Pressure Mercury Arc", Proc. Phys. Soc. B 67 (1954) pp. 768-774.

12. F. F. Chen, Introduction to Plasma Physics, Plenum Press, NY (1977).

13. I. G. Kesaev, Cathode Process in the Mercury Arc, Consultants Bureau, NY (1964).

14. R. Hancox, "Importance of Insulating Inclusions in Arc Isolation", Br. J. of Appl. Phys. 11 (1960) pp. 468-471.

15. G. Miley, "Surface Effects Related to Voltage Breakdown in CTR Devices", J. of Nucl. Mat. 63 (1976) pp. 331-336.

16. J. K. Tien, N. F. Panayotou, R. D. Stevenson, and R. A. Gross, "Unipolar Arc Damage of Materials in a Hot Dense Deuterium Plasma", J. of Nucl. Mat. 76 and 77 (1978) pp. 481-488.

17. A. E. Robson, "Report of the Ad Hoc Panel on Configurational Optimization and Impurity Control In Tokamaks", ERDA-6, Energy Research and Development Administration, June 1974.

18. Huddlestone and Leonard, Plasma Diagnostic Techniques, Plasma Research Lab, Aerospace Corp., L.A. Calif. (1968) Chap. 5.

19. W. Lochte-Holtgreven, Plasma Diagnostics, John Wiley & Sons, NY (1968).

20. J. D. Swift and M.J.R. Schwar, Electrical Probes for Plasma Diagnostics, American Elsevier Publishing Company, NY (1969).

21. W. D. Jones, A. Lee, S. M. Gleman, and H. J. Doucet, "Propagation of Ion Acoustic Waves in a Two-Electron-Temperature Plasma", Phys. Rev. Let. 35 (1975) pp. 1349-1352.

22. A. Lee, W. D. Jones, S. M. Gleman, and H. J. Doucet, "Ion-Acoustic Waves in Large Radio-Frequency Electric Fields", Phys. of Fl. 19 (1976) pp. 557-560.

23. R. E. Honig, "Vapor Pressure Data for the Solid and Liquid Elements", RCA Review 23 (Dec. 1963) pp. 567-586.

24. G. A. Farrall and G. H. Reiling, "Experimental Study of Arc Stability Part II: Investigation of Mercury Arc Stability", JAP 32 (1961) pp. 1528-1534.

25. Private Communication with Dr. G. L. Rogoff, Westinghouse R&D Center.

26. Private Communication with Dr. C. W. Kimblin, Westinghouse R&D Center.

FUSION POWER SYSTEMS
PITTSBURGH, PENNSYLVANIA

INTERNAL DOCUMENT DISTRIBUTION SHEET

REFERENCE NO: WFPS:TME-79-033
DATE: December 31, 1979
CONTRACT: EG-77-C-02-4231-A000
PROJECT/WBS CATEGORY: Student Coop Program

AUTHOR(s): C. A. Johnson
TITLE: An Experimental Study of Unipolar Arcs in a Low Pressure Mercury Discharge

APPROVAL/RELEASE CATEGORY

☐ DRAFT FOR REVIEW AND COMMENT
☐ DRAFT FOR INFORMATION ONLY
☐ PRELIMINARY RELEASE - INTERNAL PROJECT USE
☐ APPROVED BY FOR RELEASE - SUBJECT TO APPROVAL OF:

C	A	NAME
X		SHAPIRO, Z. M.
X		KLEIN, D.
X		ROSE, R. P.
X		VARLJEN, T. C.
X		FLANAGAN, C. A.
X		HALEY, T. E.
X		GIBSON, G.
X		HECK, F. M.
X		MALICK, F. S.
X		SUCOV, E. W.
	X	ALLEN, A. R.
	X	BRENNER, W. C.
	X	CHAPIN, D. L.
	X	CHI, J. W. H.
	X	CHIANESE, R. B.
	X	CROTZER, M. E.
	X	CULBERT, M. E.
	X	EASOZ, J. R.
	X	GARBER, H. J.
	X	GOLD, R. E.
	X	GREEN, L.

C	A	NAME
		HARTMAN, R. D.
	X	IBRAHIM, E. A.
	X	IWINSKI, E. M.
	X	JEDRUCH, J.
	X	KARBOWSKI, J. S.
	X	KELLY, J.
		KYSLINGER, J. A.
	X	LEE, A. Y.
	X	MARINKOVICH, P.S.
	X	MAI, L. P.
	X	MILLER, J. W.
	X	PREVENSLIK, T. V.
	X	RUCK, G. W.
	X	SCHULTZ, J. H. (MIT)
	X	SINK, D. A.
X		SMELTZER, G. S.
	X	SNIDERMAN, M.
	X	STOOKSBERRY, R. W.
X		FPS ENGINEERING OFFICE (10)

C	A	NAME
		HARDIGG, G. W. (NES)
		JONES, A. R. (AESD)
		WRIGHT, M. K. (AESD)
		CREAGAN, R. J. (R&D)
		KILGORE, L. A. (E.PGH)
		WHITNEY, E. C. (E.PGH)
		FINK, J. H. (BNL)
		KOVACIK, W. P. (R&D)
		HAUN, R. D. (R&D)
		JONES, C. K. (R&D)
		OLSEN, R. D. (R&D)
		PARKER, J. H. (R&D)
		THOMPSON, F. T. (R&D)
		WARREN, R. W. (WLASL)
		LIBERMAN, I. (WLASL)
		GROVE, D. J. (WPPPL)
		JOHNSON, J. L. (WPPPL)
		YOUNG, J. L. (R&D)
		RIEDEL, E. P. (R&D)
		HOLLAND, J. R. (R&D)
X		Carol Johnson (10)
X		Joel Falk (UOP)
X		E. E. Kintner (DOE)
X		J. F. Clarke (DOE)
X		F. E. Coffman (DOE)
X		J. F. Decker (DOE)
X		Chi. Oper. Office (6)
X		ARD Library
X		NES Library
X		~~AESD Library~~
X		R&D Library

COMMENTS

APPROVED BY:

A - ABSTRACT ONLY
C - COMPLETE COPY

REFERENCE NO: WFPS:TME-79-033
TITLE: AN EXPERIMENTAL STUDY OF UNIPOLAR ARCS IN A LOW PRESSURE MERCURY DISCHARGE
AUTHOR: C. JOHNSON